

EFFECTIVE BETA-DECAY OPERATORS WITH THE
COUPLED-CLUSTER METHOD

By

Samuel John Novario

A DISSERTATION

Submitted to
Michigan State University
in partial fulfillment of the requirements
for the degree of

Physics—Doctor of Philosophy

2017

TABLE OF CONTENTS

LIST OF TABLES	iii
LIST OF FIGURES	iv
KEY TO SYMBOLS AND ABBREVIATIONS	vii
Chapter 1 Introduction	1
1.1 A Brief History of Nuclear Structure Theory	2
1.2 Electroweak Theory and Nuclear Structure	4
1.3 Ab-Initio Descriptions of Beta Decay	6
1.4 Thesis Structure	7
Chapter 2 Many-Body Quantum Mechanics	8
2.1 Independent-Particle Model	8
2.2 Second Quantization	11
2.3 Normal Ordering	13
2.4 Wick's Theorem	15
2.5 Hartree-Fock Method	19
2.6 Configuration-Interaction	23
2.7 Many-Body Perturbation Theory	26
2.7.1 Factorization Theorem	30
Chapter 3 Coupled-Cluster Theory	32
3.1 Exponential Ansatz	32
3.1.1 The Coupled Cluster Equations	34
3.2 Linked-Cluster Theorem and MBPT	36
3.3 Example: Pairing Model	39
3.4 Solving the Coupled Cluster Equations	45
3.4.1 Symmetry Channels	46
3.4.2 Matrix Structures and Intermediates	48
3.5 Example: Homogeneous Electron Gas	51
3.6 Coupled Cluster for Finite Nuclei	57
3.6.1 Harmonic Oscillator Basis	57
3.6.2 The Nuclear Interaction	60
3.6.3 Ground-State Results for Nuclei	62
3.7 Ground-State Center-of-Mass Factorization	66
REFERENCES	71

LIST OF TABLES

LIST OF FIGURES

Figure 1.1:	Nuclear chart of nuclei with ground-state energies which have been calculated with ab-initio methods and NN+3N interactions. Figure taken from [60].	3
Figure 1.2:	Progress of ab-initio nuclear structure from calculations of ground-state energies with NN+3N interactions. Early progress was approximately linear as the problem size scaled with Moore’s law while more recent progress has taken advantage of new algorithms which have outpaced Moore’s law. Data taken from [60].	5
Figure 2.1:	A depiction of the closed-shell reference state in the independent particle model. Each horizontal line represents a shell of single-particle orbits, represented by circles, and the dotted line represents the Fermi level which separates the unoccupied <i>particle</i> states from the occupied <i>hole</i> states.	13
Figure 2.2:	A depiction of $1p-1h$, $2p-2h$, $1p-0h$, and $0p-1h$ Slater determinants defined relative to the reference state in the independent particle model. .	14
Figure 2.3:	Scaling of the matrix size and number of non-zero matrix elements for nuclear CI calculations of light nuclei. Even for modest N_{max} , the memory requirements approach the limit of petascale supercomputers (10^{10}). Figure taken from [96].	25
Figure 3.1:	Schematic representation of the pairing model space. The shells are equally spaced and doubly degenerate with one spin-up and one spin-down state.	40
Figure 3.2:	Correlation energy for the pairing model with exact diagonalization, CCD, and perturbation theory to third (MBPT3) and fourth order (MBPT4) for a range of interaction values, g	43
Figure 3.3:	Visualization of the CCD similarity transform on the pairing Hamiltonian for four particles and six shells. This shows the main function of CCD, which is to decouple $2p-2h$ excitations from the ground state, shown by the suppression of matrix elements on the first column. In the pairing model, this also has the effect of decoupling $2p-2h$ excitations from $4p-4h$ excitations. Also, the non-unitary nature of the transformation is obvious given the asymmetry of the resulting Hamiltonian.	44

Figure 3.4:	Visualization of the Fourier transform of a finite box. This transformation characterizes the construction of the single-particle basis for infinite matter, mapping plane waves in coordinate space onto finitely-spaced points in momentum space.	53
Figure 3.5:	CCD energy per electron in Hartrees for the 3D homogeneous electron gas as function of the Wigner-Seitz radius in units of Bohr radii. The calculation used periodic boundary conditions and a basis with 25 shells, resulting in a total of 1238 single-particle states. Also plotted are the variational quantum Monte Carlo (QMC) results from [75].	56
Figure 3.6:	A schematic illustration of the harmonic oscillator basis used for calculations of nuclei. Shown is an example of a initial reference state for carbon-14, with 6 protons filled to the $p3/2$ -subshell closure and 8 neutrons filled to the $p1$ -shell closure. See text for details on the single-particle states. .	58
Figure 3.7:	Diagrammatic form of the chiral EFT expansion up to $N^3\text{LO}$. The solid lines represent nucleons and the dashed lines represent pions. The different vertices represent higher-order interactions. Figure taken from [77]. .	61
Figure 3.8:	Ground-state energies for ^{16}O for the EM $N^3\text{LO}$ NN only interaction and with the added 3N interaction from Navrátil, both SRG softened with $\lambda_{\text{SRG}} = 1.88, 2.24 \text{ fm}^{-1}$. The energies are plotted for $e_{\text{max}} = 10, 12$. The most obvious difference is between the NN and NN+3N calculations, showing the importance of including 3N forces. The differences between the cutoff parameters are resolved within $\sim 1\%$ with the inclusion of 3N forces and can be rectified further by including additional correlations or full 3N forces. The experimental binding energy is shown with the grey dashed line.	64
Figure 3.9:	Ground-state energies for doubly magic nuclei as a function of the harmonic oscillator energy $\hbar\omega$ with the NN+3N(400) interaction, SRG softened with $\lambda_{\text{SRG}} = 2\text{fm}^{-1}$. The energies are plotted for $e_{\text{max}} = 8, 10, 12$, showing the convergence as the model space increases. The results are independent of the underlying oscillator frequency to $\sim 1\%$ for $e_{\text{max}} = 12$. The grey dashed line is the experimental binding energy. The overbinding of this interaction becomes apparant as the system size increases.	65
Figure 3.10:	Ground-state energies for singly magic nuclei as a function of the harmonic oscillator energy $\hbar\omega$ with the NN+3N(400) interaction, SRG softened with $\lambda_{\text{SRG}} = 2\text{fm}^{-1}$. The energies are plotted for different e_{max} . The results are independent of the underlying oscillator frequency to $\sim 1\%$ for $e_{\text{max}} = 12$. The grey dashed line is the experimental binding energy. These results underbind with respect to their doubly-magic counterparts in Fig. 3.9.	66

Figure 3.11: Ground-state COM energies, Eq. (3.56), for ^{16}O and ^{40}Ca at varies harmonic oscillator frequencies with the NN+3N(400)-induced with $\lambda_{\text{SRG}} = 2.0 \text{ fm}^{-1}$ at $e_{\text{max}} = 12$. Using the proper COM oscillator frequencies shows the approximate factorization of Eq. (3.55). 70

KEY TO SYMBOLS AND ABBREVIATIONS

$Ap-Bh$ A -particle, B -hole excitation or de-excitation from the reference state

$|0\rangle$ vacuum state

$|\Phi_0\rangle$ reference state

$|\Psi\rangle$ correlated ground state

$|\Phi_{i_1 \dots i_B}^{a_1 \dots a_A}\rangle$ specific $Ap-Bh$ state

$\{\dots\}$ normal-ordered with respect to the reference state

$\hbar\omega$ harmonic oscillator energy scale

\hat{H} Hamiltonian

\bar{H} similarity-transformed Hamiltonian

\hat{H}_N normal-ordered Hamiltonian

\bar{H}_N normal-ordered similarity-transformed Hamiltonian

\hat{T} cluster operator

$\varepsilon_{i_1 \dots i_B}^{a_1 \dots a_A}$ energy denominator, $f_{i_1}^{i_1} + \dots + f_{i_B}^{i_B} - f_{a_1}^{a_1} - \dots - f_{a_A}^{a_A}$

CC coupled cluster

CCD coupled cluster with doubles

CCSD coupled cluster with singles and doubles

CCSDT coupled cluster with singles, doubles, and triples

CCSD(T) coupled cluster with singles, doubles, and triples approximation

Λ -CCSD(T) coupled cluster with singles, doubles, and Λ -triples approximation

CI configuration interaction

FCI full configuration interaction

COM center of mass

EOM equations-of-motion

PA particle-attached

PR particle-removed
EOM equations-of-motion
EOM-CC equations-of-motion coupled cluster
EOM-CCSD equations-of-motion coupled cluster with singles and doubles
HF Hartree-Fock
IM-SRG in-medium similarity renormalization group
HO harmonic oscillator
LECs low-energy constants
MBPT many-body perturbation theory
WS Woods-Saxon
DIIS direct-inversion of the iterative subspace
QCD quantum chromodynamics
EFT effective field theory
NN nucleon-nucleon
3N three-nucleon
NLO next-to leading order
N²LO next-to-next-to leading order
N³LO next-to-next-to-next-to leading order

Chapter 1

Introduction

Steady progress in any modern scientific endeavor requires a strong, dynamic relationship between experimental data to paint an accurate picture of some natural phenomena and theoretical models to interpret those phenomena with respect to the growing network of other scientific models. Conversely, the predictive capability of theoretical models can highlight blurry or unfinished areas of that picture which can be clarified or completed by new or improved experimental techniques. In the pursuit to understand and describe the atomic nucleus and the corresponding implications from quarks to neutron stars, this push-and-pull coordination between theory and experiment makes progress in modern nuclear physics robust and persistent.

An integral component of modern nuclear physics is describing the structure and emergent properties of self-bound systems of protons and neutrons. The systems in questions can be stable nuclei, rare isotopes far from stability, and even infinite nuclear matter which can be used to model neutron stars. Relevant properties to nuclear structure include ground-state energies—for determining nuclear masses, excited-state energies—for identification in gamma or neutron spectroscopy, and transition or decay amplitudes—for calculating the respective rates for those processes. This wide array of emergent properties inserts both nuclear structure theory and experiment into a prominent role within every other subfield of modern nuclear physics, from lattice quantum chromodynamics (QCD) to nuclear astrophysics, and beyond, to questions about fundamental symmetries and dark matter. However, two inextricable characteristics of a comprehensive model of nuclear structure—the increasingly large

size of many-body nuclear systems and the complexity and strength of the nucleon-nucleon interactions—have been imposing hurdles for theorists to overcome.

1.1 A Brief History of Nuclear Structure Theory

The project to solve the correlation problem in many-fermion systems began with the work of Brueckner, Bethe, and Goldstone [22, 11, 1] with the reformulation of the nuclear interaction by accounting for two-body correlations from the nuclear medium. This work continued with the work of Coester and Kummel [30, 31, 71] with a further resummation of nuclear correlations in the form of an exponential ansatz into what would become coupled-cluster (CC) theory. However, there were two major obstacles that hindered the progress in this area for decades. First, while these methods were systematically improvable by including progressively higher-level correlations, the highly-nonperturbative nature of the nuclear force required computationally infeasible summations. Second, there wasn't a reliable and consistent theory to model nucleon-nucleon interactions.

However, the well-known and highly-perturbative Coulomb force, which underlies the many-electron systems in atoms and molecules, made consistent advances in ab-initio quantum chemistry possible since the 1950s. Along with the quasi-exact method of configuration interaction (CI) [99, 32, 4, 117] which physicists have utilized since the formulation of quantum mechanics, chemists successfully employed approximate methods like many-body perturbation theory (MBPT) [62, 63, 95, 97] and coupled-cluster theory [28, 26, 27, 87, 97].

Fortunately, within the past decade, two breakthroughs have allowed ab-initio nuclear structure to resurface and thrive the way that quantum chemistry had done in the previous decades. First was the invention of chiral effective field theory (EFT) [39, 76] which gave theorists the ability to construct nucleon-nucleon interactions consistent with the underlying

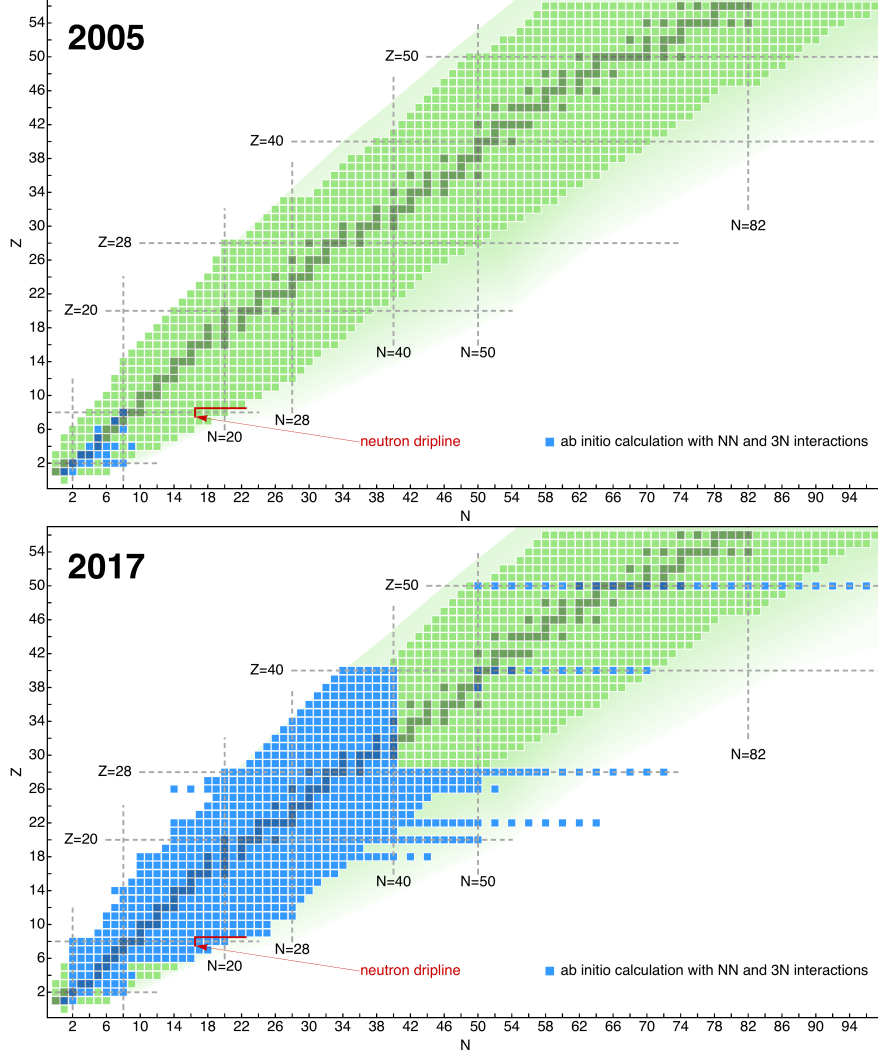


Figure 1.1: Nuclear chart of nuclei with ground-state energies which have been calculated with ab-initio methods and NN+3N interactions. Figure taken from [60].

QCD of the strong nuclear force. Second was the application of renormalization group (RG) methods to the nuclear force [17, 94]. This procedure can “soften” the NN interaction, to decouple the high- and low-momentum components of the nuclear force and generate less-correlated systems that can be calculated at a reasonable computational cost. These major changes to nuclear structure theory made it possible to merge the field with the progress of quantum chemistry and open a new area for additional developments in ab-initio descriptions of many-fermion systems, see Fig. 1.1.

Along with exponential improvements to high-performance computing, these novel techniques have allowed modern many-body methods to extend their reach and deepen their applicability across the nuclear chart, see Fig. 1.2. The no-core shell model (NCSM), a quasi-exact method, has been able to reach the *sd* shell and useful in calculating the radii, transition strengths, and effective interactions of light nuclei [83, 84, 6]. Another quasi-exact technique which follows a completely different methodology than NCSM, quantum Monte Carlo (QMC), has also progressed and is now capable of calculating properties of light nuclei with modern chiral forces [89, 88, 25]. In addition to these exponentially scaling techniques' successes with lighter nuclei, polynomially scaling techniques—such as the in-medium similarity renormalization group (IMSRG) [115, 116, 58, 15, 59, 57, 105, 104], self-consistent Green's functions (SCGF) [101, 102, 103], and coupled cluster theory [123, 124, 65, 66, 51, 70, 47, 12]—have been able to reach open-shell nuclei through the *pf* shell and even up to the chain of even tin isotopes with equations-of-motion and multi-reference techniques.

1.2 Electroweak Theory and Nuclear Structure

Nuclear structure is implicated in performing and analyzing experiments to probe fundamental symmetries and physics beyond the Standard Model. One example is determining the V_{ud} component of the Cabbibo-Kobayashi-Maskawa (CKM) matrix, which relates quark eigenstates of the weak interaction to their mass eigenstates [24, 68]. This matrix element can be determined from by measuring the half-lives of superallowed Fermi beta decays [110] and applying a nucleus-dependent structure correction [111, 114, 113, 5, 67]. The value of $|V_{ud}|$ is used to test the unitarity of the CKM matrix and the conserved-vector current hypothesis, which relates the ft -values of superallowed Fermi beta decays of different nuclei, both predicted by the standard model [54].

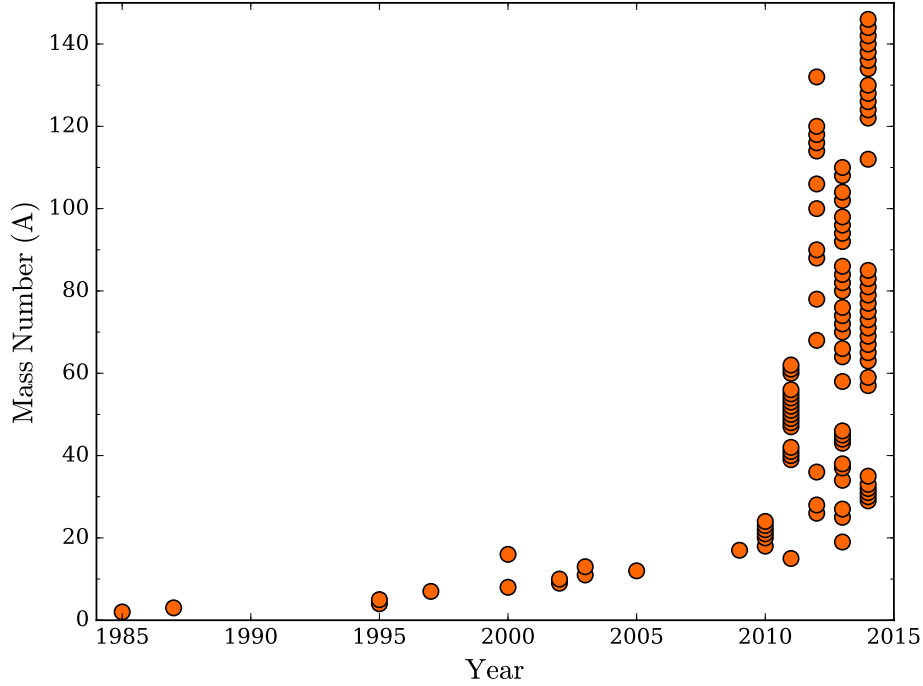


Figure 1.2: Progress of ab-initio nuclear structure from calculations of ground-state energies with NN+3N interactions. Early progress was approximately linear as the problem size scaled with Moore’s law while more recent progress has taken advantage of new algorithms which have outpaced Moore’s law. Data taken from [60].

Another example of physics beyond the standard model is the neutrinoless double-beta decay ($0\nu\beta\beta$) [106, 3]. The extremely-rare, two-neutrino double-beta decay ($2\nu\beta\beta$) has been observed in many experiments [36, 79], which has motivated the search for its neutrinoless counterpart, in which two Majorana neutrinos—being their own antiparticles—annihilate one another, which is not possible in the standard electro-weak theory. The long half-lives of these theoretical decays depend on a phase-space factor, which is highly dependent on the decay Q -value, and a nuclear matrix element. The Q -value can be determined from high-precision mass measurements of the relevant nuclei [73, 49, 92, 23], while the nuclear matrix element, which contributes the largest source of uncertainty, must be calculated with a sufficient many-body theory.

The weak interaction and nuclear structure can also be exploited for supernova neutrino

detection and spectroscopy. While these original detectors were based on electron-neutrino scattering [61, 13], more recent experiments utilize correlated nucleon effects of large nuclei to enhance the scattering cross section and therefore the ability to resolve energies and distinguish neutrino flavors [55, 29, 41, 72]. Supernova models predict distinct distributions for different neutrino flavors based on the temperatures at which they are emitted [69, 9]. With nuclear structure calculations that include sufficient nuclear correlations, these high-resolution detectors can be used to verify specific models.

1.3 Ab-Initio Descriptions of Beta Decay

Since Enrico Fermi’s originally rejected paper describing β decay in 1934 [42, 122], theorists have worked to refine this description within the ever-growing library of knowledge concerning the nature of the weak force, the characteristics of the neutrino, and the structure of nuclei. With the success of ab-initio calculations for nuclear properties such as masses, radii, and electromagnetic phenomena, these techniques also seem promising ways to calculate relevant quantities involved in nuclear β decay. Because the kinematics of the decay and the underlying weak process are well understood, the remaining task for nuclear theory to tackle is calculating the transition amplitudes between the initial and final nuclei.

Modern calculations of these β -decay matrix elements were originally performed using phenomenological interactions in the shell model framework [121, 20, 119, 86]. Also, predecessors to current ab-initio techniques like the random-phase approximation (RPA) [112] included core-correlation effects in these early descriptions. These methods were able to successfully reproduce experimental lifetime data and address technical issues such as the quenching of the axial-vector coupling constant. More recently, the success of the shell model has inspired an extension to the new method, known as the ab-initio shell model, where an

effective interaction is constructed within a certain valence space using a many-body method such as CC [35] or IMSRG [16]. However, these techniques are computationally expensive and cannot currently reach heavy nuclei of interest. The most common method used in their place is known as the quasiparticle random-phase approximation (QRPA) [107, 37]. While these calculations can be performed for heavy nuclei in large spaces, they also rely on phenomenological effective interactions. Therefore, there is a demand for computationally-economical, ab-initio techniques that can capture the relevant many-body correlations needed to accurately describe the nuclear structure aspects of electro-weak processes.

1.4 Thesis Structure

The main goal of this work is to explore the ab-initio description of nuclear beta decay within the coupled-cluster theory framework of EOM-CCSD using renormalized chiral NN and 3N interactions. The organization of the thesis builds from a general description of the many-body problem of quantum mechanics in chapter 2. Then, in chapter 3, this many-body framework is applied within the coupled-cluster theory and applied to various systems including atomic nuclei. In chapter ??, coupled-cluster theory is extended to the equations-of-motion method to describe open-shell systems. Chapter ?? outlines the procedure to express observables as effective coupled-cluster operators and how to calculate those observables in the equations-of-motion framework. Then, in chapter ??, the ability to calculate effective operators is applied to Fermi- and Gamow-Teller- beta-decay operators and relevant quantities are determined for various nuclei. Lastly, conclusions and future perspectives are given in chapter ?? while technical details concerning the formalism and implementation are given in the appendix ??.

Chapter 2

Many-Body Quantum Mechanics

Ab-initio structure calculations of many-fermion systems such as those in nuclear and electronic structure aim to describe emergent phenomena from the constituent particles subject to the underlying microscopic Hamiltonian. This amounts to finding the solution to the many-body Schrödinger equation. However, a calculation of the exact solution needs to account for all possible correlations among the particles and thus scales factorially. This motivates the need for approximations to the exact solution that account for the most important correlations. This chapter first establishes the formalism necessary to define the many-body problem then illustrates several successive approximations to its solution. Because the type of fermions and the underlying Hamiltonian can be kept generic until specific systems are considered, the formalism and many-body methods can be kept generic as well.

2.1 Independent-Particle Model

The nonrelativistic A-body quantum problem begins with the Schrödinger equation,

$$\hat{H}\Psi_{\nu}(\mathbf{r}_1, \dots, \mathbf{r}_A) = E_{\nu}\Psi_{\nu}(\mathbf{r}_1, \dots, \mathbf{r}_A), \quad (2.1)$$

for the correlated wave function $\Psi_{\nu}(\mathbf{r}_1, \dots, \mathbf{r}_A)$ and the corresponding energy E_{ν} . The Hamiltonian can be written generically as a sum of k -body pieces which, in principle, can

contain up to A -body interactions,

$$\begin{aligned}\hat{H} &= {}^{(1)}\hat{H} + {}^{(2)}\hat{H} + {}^{(3)}\hat{H} + \dots \\ &= \sum_i^A {}^{(1)}\hat{H}(\mathbf{r}_i) + \sum_{i<j}^A {}^{(2)}\hat{H}(\mathbf{r}_i, \mathbf{r}_j) + \sum_{i<j<k}^A {}^{(3)}\hat{H}(\mathbf{r}_i, \mathbf{r}_j, \mathbf{r}_k) + \dots\end{aligned}\quad (2.2)$$

Regardless of the system, the one-body term contains the kinetic energy operator $\frac{\hbar^2}{2m}\nabla_i^2$, while the higher-order terms result from inter-particle interactions.

An intuitive way to formulate the solution to the many-body Schrödinger equation is to express the collective wave function in terms of independent single-particle wave functions, or orbitals $\phi(\mathbf{r})$. In this *independent-particle model*, a selection of single-particle wave functions, known as the single-particle basis, are constructed by solving the Schrödinger equation for a single particle in some mean-field potential, for bound systems, or in free space, for infinite systems. Then a many-body wave function is constructed as a product of these single-particle orbits. This simple model is justified because it becomes exact when inter-particle interactions are completely suppressed and is useful because it provides an intuitive way to interpret complicated many-body dynamics as processes involving few single-particle wave functions.

A many-body wave function of fermions must be anti-symmetric with respect to particle exchange so that the Pauli exclusion principle is followed, such that no single-particle wave function is occupied by more than one fermion. This condition is satisfied by a wave function

in the form of a *Slater determinant* [100],

$$\Phi(\mathbf{r}_1, \dots, \mathbf{r}_A) = \frac{1}{\sqrt{A!}} \begin{vmatrix} \phi_1(\mathbf{r}_1) & \phi_1(\mathbf{r}_2) & \cdots & \phi_1(\mathbf{r}_A) \\ \phi_2(\mathbf{r}_1) & \phi_2(\mathbf{r}_2) & \cdots & \phi_2(\mathbf{r}_A) \\ \vdots & \vdots & \ddots & \vdots \\ \phi_A(\mathbf{r}_1) & \phi_A(\mathbf{r}_2) & \cdots & \phi_A(\mathbf{r}_A) \end{vmatrix}, \quad (2.3)$$

where A is the number of particles in the system and $\phi_p(\mathbf{r}_\mu)$ is the p -th orbital filled with the μ -th particle.

If the orbitals are constructed from an appropriate phenomenological potential, a Slater determinant composed of the A lowest orbitals can represent a fairly good approximation to the ground state for a closed-shell system, where the lowest-energy Slater determinant can be uniquely determined. The set of all Slater determinants in a certain model space of single-particle wave functions defines a complete A -body Hilbert space such that a generic wave function can be written as a linear combination of Slater determinants,

$$\Psi_\nu(\mathbf{r}_1, \dots, \mathbf{r}_A) = \sum_{\mu=1}^{\mathcal{N}} C_\nu^\mu \Phi_\mu(\mathbf{r}_1, \dots, \mathbf{r}_A), \quad (2.4)$$

where $C_\nu^\mu = \langle \Psi(\mathbf{r}_1, \dots, \mathbf{r}_A) | \Phi_\nu^\mu(\mathbf{r}_1, \dots, \mathbf{r}_A) \rangle$. The number of Slater determinants \mathcal{N} in an A -body Hilbert space with N orbits is given by,

$$\mathcal{N} = \binom{N}{A} = \frac{N!}{A!(N-A)!}, \quad (2.5)$$

which shows the factorial scaling of the exact problem. However, to reduce the size of the problem, progressively more significant Slater determinants can be chosen to systematically

refine approximations to the full solution.

2.2 Second Quantization

Even with the simplification of the independent-particle model, the many-body Schrödinger equation is an unwieldy and complex system of coupled differential equations. A useful reformulation of this equation is to promote the single-particle orbits to operators in a step known as *second quantization* (see e.g., [97, 43]). In this framework, a Slater determinant is represented by a string of occupied orbitals,

$$\Phi(\mathbf{r}_1, \dots, \mathbf{r}_A) \equiv \mathcal{A} \left(\phi_{p_1} \phi_{p_2} \phi_{p_3} \cdots \phi_{p_N} \right) \equiv |p_1 p_2 p_3 \cdots p_N\rangle, \quad (2.6)$$

where \mathcal{A} represents a permutation and normalization operator to correspond with Eq. (2.3). These second-quantized Slater determinants can be constructed with the use of operators that correspond to specific orbitals. A *creation* operator, \hat{a}_p^\dagger , places a particle in the p orbital, and an *annihilation* operator, \hat{a}_p , removes a particle from the p orbital,

$$\hat{a}_p^\dagger |0\rangle = |p\rangle \quad \hat{a}_p |p\rangle = |0\rangle, \quad (2.7)$$

where $|0\rangle$ represents the true vacuum, a state void of any particles. Because there must be a correspondence between the original first quantization and second quantization, these creation and annihilation operators obey the following anticommutation relations ($[\hat{A}, \hat{B}]_+ = \hat{A}\hat{B} + \hat{B}\hat{A}$),

$$[\hat{a}_p^\dagger, \hat{a}_q]_+ = \delta_{pq} \quad [\hat{a}_p^\dagger, \hat{a}_q^\dagger]_+ = [\hat{a}_p, \hat{a}_q]_+ = 0, \quad (2.8)$$

which guarantee that wave functions comprised of these operators obey antisymmetry and the Pauli exclusion principle required of fermionic systems.

The Hamiltonian in the form of Eq. (2.2) can be written with second-quantized operators as,

$$\hat{H} = \sum_{pq} {}^{(1)}H_q^p \hat{a}_p^\dagger \hat{a}_q + \frac{1}{4} \sum_{pqrs} {}^{(2)}H_{rs}^{pq} \hat{a}_p^\dagger \hat{a}_q^\dagger \hat{a}_s \hat{a}_r + \frac{1}{36} \sum_{pqrstu} {}^{(3)}H_{stu}^{pqr} \hat{a}_p^\dagger \hat{a}_q^\dagger \hat{a}_r^\dagger \hat{a}_u \hat{a}_t \hat{a}_s + \dots, \quad (2.9)$$

where the prefactors account for the double counting of particle-particle interactions, and the matrix elements represent integrals over the relevant single-particle wave functions,

$$\begin{aligned} {}^{(1)}H_q^p &\equiv \int d\mathbf{r}_1 \phi_p^*(\mathbf{r}_1) {}^{(1)}\hat{H}(\mathbf{r}_1) \phi_q(\mathbf{r}_1) \\ {}^{(2)}H_{rs}^{pq} &\equiv \int d\mathbf{r}_1 d\mathbf{r}_2 \phi_p^*(\mathbf{r}_1) \phi_q^*(\mathbf{r}_2) {}^{(2)}\hat{H}(\mathbf{r}_1, \mathbf{r}_2) [\phi_r(\mathbf{r}_1) \phi_s(\mathbf{r}_2) - \phi_s(\mathbf{r}_1) \phi_r(\mathbf{r}_2)] \\ &\vdots \end{aligned} \quad (2.10)$$

Matrix elements involving two or more particles include exchange terms which guarantee that they are also antisymmetric,

$$\begin{aligned} {}^{(2)}H_{rs}^{pq} &= -{}^{(2)}H_{rs}^{qp} = -{}^{(2)}H_{sr}^{pq} = {}^{(2)}H_{sr}^{qp} \\ {}^{(3)}H_{stu}^{pqr} &= -{}^{(3)}H_{stu}^{qpr} = -{}^{(3)}H_{tsu}^{pqr} = {}^{(3)}H_{tsu}^{qpr} = \dots \end{aligned} \quad (2.11)$$

These definitions apply regardless of the form of the Hamiltonian, and thus this formalism remains generic to the particular system. Second quantization is a crucial step in simplifying the many-body Schrödinger equation because it reduces the complexity of the spatial and spin degrees of freedom within the single-particle wave functions and interactions into precomputed matrix elements. The remaining effort is reduced to algebraic expressions in-

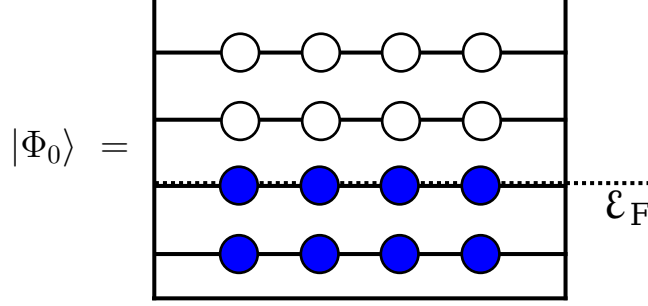


Figure 2.1: A depiction of the closed-shell reference state in the independent particle model. Each horizontal line represents a shell of single-particle orbits, represented by circles, and the dotted line represents the Fermi level which separates the unoccupied *particle* states from the occupied *hole* states.

volving creation and annihilation operators.

2.3 Normal Ordering

It's convenient to define an A-particle reference state, where states are filled from the true vacuum up to a closed shell, known as the Fermi level. This reference state must be uniquely determined from the number of particles in the system and therefore nondegenerate with other Slater determinants,

$$|\Phi_0\rangle = \left\{ \prod_i^A \hat{a}_i^\dagger \right\} |0\rangle. \quad (2.12)$$

This reference determinant defines a new *Fermi vacuum*. States above the Fermi vacuum are called *particle* states and will be denoted with the indices a, b, c, d, \dots while states below the Fermi vacuum are called *hole* states and will be denoted with the indices i, j, k, l, \dots . Generic states above or below the Fermi vacuum will be denoted with the indices p, q, r, s, \dots .

Any other Slater determinant can be constructed relative to this reference state by adding particles and/or removing holes. A Slater determinant with A particles added and B holes

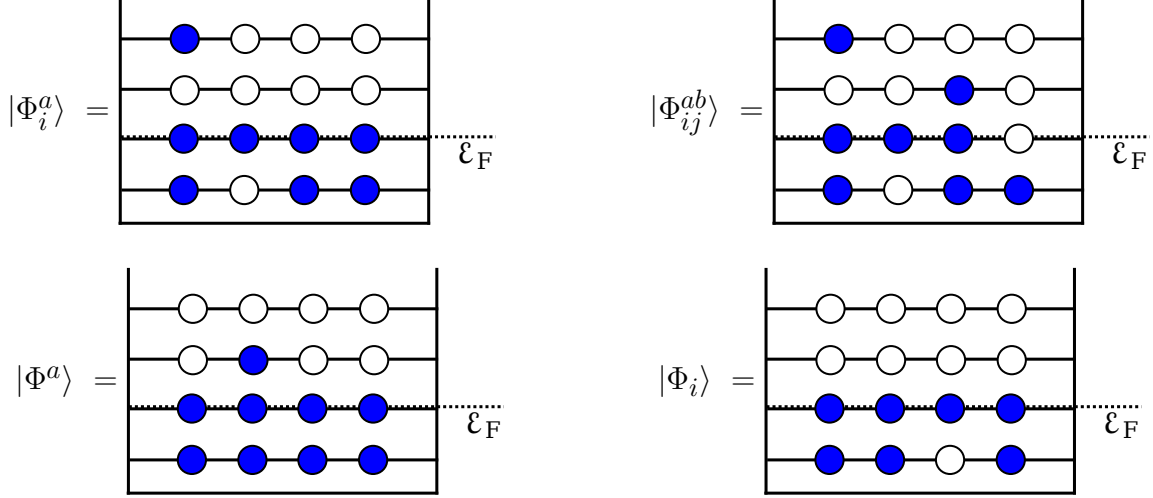


Figure 2.2: A depiction of $1p-1h$, $2p-2h$, $1p-0h$, and $0p-1h$ Slater determinants defined relative to the reference state in the independent particle model.

removed from reference state is known as a $Ap-Bh$ excitation.

$$\begin{aligned}
 |\Phi_i^a\rangle &\equiv \hat{a}_a^\dagger \hat{a}_i |\Phi\rangle \\
 |\Phi_{ij}^{ab}\rangle &\equiv \hat{a}_a^\dagger \hat{a}_b^\dagger \hat{a}_j \hat{a}_i |\Phi\rangle \\
 |\Phi^a\rangle &\equiv \hat{a}_a^\dagger |\Phi\rangle \\
 |\Phi_i\rangle &\equiv \hat{a}_i |\Phi\rangle
 \end{aligned} \tag{2.13}$$

Using these definitions, hole-creation and particle-annihilation operators vanish when acting on the Fermi vacuum from the left, $\hat{a}_i^\dagger |\Phi_0\rangle = \hat{a}_a |\Phi_0\rangle = 0$. Conversely, hole-annihilation and particle-creation operators vanish when acting on the Fermi vacuum from the right, $\langle \Phi_0 | \hat{a}_i = \langle \Phi_0 | \hat{a}_a^\dagger = 0$.

These results can be exploited to simplify expressions involving strings of creation and annihilation operators by a procedure called *normal ordering* with respect to the Fermi vacuum. Denoted by $\{\cdots\}$, normal ordering permutes a string of creation and annihilation operators so that hole-annihilation and particle-creation operators are to the left of hole-

creation and particle-annihilation operators, which guarantees that normal ordered operators vanish on the Fermi vacuum, $\langle \Phi_0 | \{ \dots \} = 0$ and $\{ \dots \} | \Phi_0 \rangle = 0$.

$$\left\{ \hat{a}_j^\dagger \cdots \hat{a}_i \cdots \hat{a}_b \cdots \hat{a}_a^\dagger \right\} = (-1)^\sigma \hat{a}_i \cdots \hat{a}_a^\dagger \cdots \hat{a}_j^\dagger \cdots \hat{a}_b, \quad (2.14)$$

where σ is the number of two-state permutations required to do the normal ordering.

2.4 Wick's Theorem

At this point, the many-body problem has been reduced to computing long strings of creation and annihilation operators between the normal-ordered Hamiltonian and the correlated wave function using Eq. (2.8). Instead of using a brute-force approach by permuting over and over, a further simplification known as *Wick's theorem* [120] can be introduced. A Wick contraction of two operators with respect to the reference state is defined as

$$\overline{\hat{A}\hat{B}} = \hat{A}\hat{B} - \left\{ \hat{A}\hat{B} \right\}. \quad (2.15)$$

Which, given the definition in Eq. (2.14) and the anticommutation relations in Eq. (2.8), means that the only nonzero contractions are of the form,

$$\overline{\hat{a}_i^\dagger \hat{a}_j} = \delta_{ij} \quad \text{and} \quad \overline{\hat{a}_a \hat{a}_b^\dagger} = \delta_{ab}. \quad (2.16)$$

Because contracted operators simply represent a Kronecker delta, they can be removed from a normal ordered product by permuting the product σ times so that the contracted operators

are next to each other,

$$\{\hat{A} \cdots \overbrace{\hat{B} \cdots \hat{C}} \cdots \hat{D}\} = (-1)^\sigma \{\hat{A} \cdots \overbrace{\hat{B} \hat{C}} \cdots \hat{D}\} = (-1)^\sigma \overbrace{\hat{B} \hat{C}} \{\hat{A} \cdots \hat{D}\}. \quad (2.17)$$

These different definitions for operator manipulation come together to define the time-independent Wick's theorem, which reformulates a product of operators as the sum of its normal-ordered form and all possible contractions of its normal-ordered form.

$$\hat{A} \hat{B} \hat{C} \cdots = \left\{ \hat{A} \hat{B} \hat{C} \cdots \right\} + \sum_{\substack{\text{one-} \\ \text{contractions}}} \left\{ \overbrace{\hat{A} \hat{B} \hat{C} \cdots} \right\} + \sum_{\substack{\text{two-} \\ \text{contractions}}} \left\{ \overbrace{\overbrace{\hat{A} \hat{B} \hat{C} \cdots}} \right\} + \cdots + \sum_{\substack{\text{all-} \\ \text{contractions}}} \left\{ \overbrace{\overbrace{\overbrace{\hat{A} \hat{B} \hat{C} \cdots}}} \right\} \quad (2.18)$$

Wick's theorem is incredibly useful in many-body techniques because complicated expressions of operators can be expressed as diagrams that are easy to compute with simple diagrammatic rules which correspond to Eqs. (2.8), (2.16), and (2.17). These diagrammatic techniques are an integral component to deriving expressions used in this work, and their underlying rules are summarized in ?? and are extensively discussed in [97].

A powerful application of Wick's theorem is to rewrite the Hamiltonian in normal-ordered form.

$$\hat{H} = E_0 + \sum_{pq} f_q^p \left\{ \hat{a}_p^\dagger \hat{a}_q \right\} + \frac{1}{4} \sum_{pqrs} V_{rs}^{pq} \left\{ \hat{a}_p^\dagger \hat{a}_q^\dagger \hat{a}_s \hat{a}_r \right\} + \frac{1}{36} \sum_{pqrstu} W_{stu}^{pqr} \left\{ \hat{a}_p^\dagger \hat{a}_q^\dagger \hat{a}_r^\dagger \hat{a}_u \hat{a}_t \hat{a}_s \right\} + \cdots, \quad (2.19)$$

where the newly defined normal-ordered Hamiltonian terms are defined as,

$$\begin{aligned}
E_0 &= \text{diagram with a circle and an incoming line labeled } i \text{ meeting a dashed line with a cross} + \text{diagram with two circles and incoming lines } i, j \text{ meeting a dashed line} + \text{diagram with three circles and incoming lines } i, j, k \text{ meeting a dashed line} + \dots \\
&= \sum_i {}^{(1)}H_i^i + \frac{1}{2} \sum_{ij} {}^{(2)}H_{ij}^{ij} + \frac{1}{6} \sum_{ijk} {}^{(3)}H_{ijk}^{ijk} \dots
\end{aligned} \tag{2.20}$$

$$\begin{aligned}
\text{diagram with two incoming lines } p, q \text{ meeting a dashed line with a cross} &= \text{diagram with two incoming lines } p, q \text{ meeting a dashed line} + \text{diagram with two incoming lines } p, q \text{ meeting a dashed line and a circle with an incoming line } i \text{ attached} + \text{diagram with two incoming lines } p, q \text{ meeting a dashed line and two circles with incoming lines } i, j \text{ attached} + \dots \\
f_q^p &= {}^{(1)}H_q^p + \sum_i {}^{(2)}H_{qi}^{pi} + \frac{1}{2} \sum_{ij} {}^{(3)}H_{qij}^{pij} + \dots
\end{aligned} \tag{2.21}$$

$$\begin{aligned}
\text{diagram with two vertices connected by a dashed line, each with two incoming lines } (p, r) \text{ and } (q, s) &= \text{diagram with two vertices connected by a dashed line, each with two incoming lines } (p, r) \text{ and } (q, s) + \text{diagram with two vertices connected by a dashed line, each with two incoming lines } (p, r) \text{ and } (q, s) \text{ and a circle with an incoming line } i \text{ attached to the second vertex} + \dots \\
V_{rs}^{pq} &= {}^{(2)}H_{rs}^{pq} + \sum_i {}^{(3)}H_{rsi}^{pqi} + \dots
\end{aligned} \tag{2.22}$$

$$\begin{aligned}
\text{diagram with two vertices connected by a dashed line, each with two incoming lines } (p, s) \text{ and } (q, t) \text{ on the left, and } (r, u) \text{ on the right} &= \text{diagram with two vertices connected by a dashed line, each with two incoming lines } (p, s) \text{ and } (q, t) \text{ on the left, and } (r, u) \text{ on the right} + \dots \\
W_{stu}^{pqr} &= {}^{(3)}H_{stu}^{pqr} + \dots
\end{aligned} \tag{2.23}$$

This has the effect of shuffling higher-order interactions into lower-order terms, and makes it feasible to include computationally expensive many-body interactions as normal-ordered few-body interactions. Also, it reorganizes many-body correlations into the reference state so that additional correlations around the Fermi surface can be treated as a perturbation. Therefore, from this point forward, the many-body problem will be formulated in terms of the normal-ordered Hamiltonian, and the bare interactions will be truncated beyond the three-body level for computational feasibility. Electronic systems are naturally truncated at the two-body Coulomb force, while nuclear systems can be successfully described with the two-body normal-ordered piece of the three-body force.

In this form, the Hamiltonian is written as a sum of the *reference energy*, E_0 , which is the fully-contracted expectation value of the Hamiltonian with respect to the reference state,

$$E_0 = \langle \Phi | \hat{H} | \Phi \rangle, \quad (2.24)$$

and the remaining normal-ordered pieces of the Hamiltonian, \hat{H}_N . Rewriting the many-body Schrödinger equation for the ground state, $|\Psi\rangle$, and using this partition gives,

$$\begin{aligned} \hat{H}|\Psi\rangle &= (E_0 + \hat{H}_N)|\Psi\rangle = E|\Psi\rangle \\ \longrightarrow \hat{H}_N|\Psi\rangle &= (E - E_0)|\Psi\rangle = \Delta E|\Psi\rangle, \end{aligned} \quad (2.25)$$

where ΔE is known as the *correlation energy*.

Now that the many-body quantum problem has been formulated, different approaches to solving that problem can be proposed and analyzed. Because taking account of correlations from all particles simultaneously is a demanding—and for some systems, computationally impossible—endeavor, methods for solving the many-body Schrödinger equation should be

systematically improvable. Successful methods with this quality incorporate the most dominant correlations in lower-order solutions and approach the exact solution when more and more orders are included.

2.5 Hartree–Fock Method

A successful, first-order approximation to any many-body method comes from noticing that each individual particle feels a mean-field potential from the cumulative interactions with all the other particles. The *Hartree-Fock* (HF) method [56, 44] aims to transform the original single-particle basis to a Hartree-Fock basis where each orbital is the eigenfunction of its corresponding mean-field. Because the transformation of a single orbital changes its effect on every other particle, this process must be performed iteratively until self-consistency between all the orbitals is reached, which is why this method is also known as the *Self-Consistent Field* (SCF) method.

This mean-field picture results from the following procedure. It begins by minimizing the reference energy with respect to the reference state. This functional is just the zero-body piece of the normal-ordered Hamiltonian,

$$E_{\text{HF}}[\Phi_0] = \langle \Phi_0 | \hat{H} | \Phi_0 \rangle = \sum_i {}^{(1)}H_i^i + \frac{1}{2} \sum_{ij} {}^{(2)}H_{ij}^{ij} + \frac{1}{6} \sum_{ijk} {}^{(3)}H_{ijk}^{ijk}. \quad (2.26)$$

Transforming the reference determinant can be accomplished by rotating the state within the single-particle basis by use of the *Thouless theorem* [109], which states that any Slater determinant can be written as the product of any other Slater determinant and an exponentiated

single-excitation operator,

$$|\Phi'\rangle = e^{\hat{C}_1} |\Phi_0\rangle, \quad \text{where } \hat{C}_1 = \sum_{ai} C_i^a \{ \hat{a}_a^\dagger \hat{a}_i \}. \quad (2.27)$$

If the difference between the two Slater determinants is dominated by single excitations, this transformation can be approximated by expanding the exponential and ignoring higher-order terms,

$$|\Phi'\rangle \simeq \left(1 + \sum_{ai} C_i^a \{ \hat{a}_a^\dagger \hat{a}_i \} \right) |\Phi_0\rangle. \quad (2.28)$$

The reference energy functional can now be written as a sum of the original reference state and new terms that incorporate the single-excitation variation,

$$E_{\text{HF}} [\Phi'] = \langle \Phi' | \hat{H} | \Phi' \rangle \simeq E_{\text{HF}} [\Phi_0] + \sum_{ai} C_i^a \langle \Phi_0 | \hat{H} | \Phi_i^a \rangle + \sum_{ai} C_i^{a*} \langle \Phi_i^a | \hat{H} | \Phi_0 \rangle. \quad (2.29)$$

The minimum of this functional is found by differentiating the expression with respect to the coefficients C_i^a and setting the result to zero,

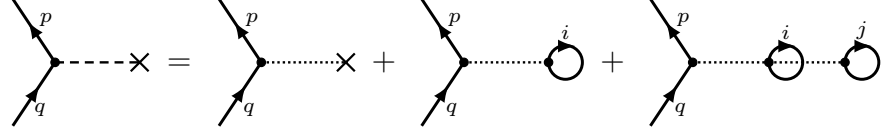
$$\delta E_{\text{HF}} [\Phi'] \simeq \sum_{ai} \delta C_i^a \langle \Phi_0 | \hat{H} | \Phi_i^a \rangle + \sum_{ai} \delta C_i^{a*} \langle \Phi_i^a | \hat{H} | \Phi_0 \rangle = 0 \quad (2.30)$$

Because this expression is Hermitian, both terms must vanish independently so that,

$$\langle \Phi_0 | \hat{H} | \Phi_i^a \rangle = \langle \Phi_i^a | \hat{H} | \Phi_0 \rangle = 0. \quad (2.31)$$

This condition is the result of the *Brillouin theorem* [19], which states that the Hamiltonian matrix element must vanish between an optimized Hartree-Fock ground state and any single excitation from it. The Brillouin condition is satisfied by diagonalizing the one-body piece

of the normal-ordered Hamiltonian f_q^p , known as the *Fock* operator, such that off-diagonal pieces like $\langle \Phi_0 | \hat{H} | \Phi_i^a \rangle = f_a^i$ and $\langle \Phi_i^a | \hat{H} | \Phi_0 \rangle = f_i^a$ vanish.



$$f_q^p = {}^{(1)}H_q^p + \sum_i {}^{(2)}H_{qi}^{pi} + \frac{1}{2} \sum_{ij} {}^{(3)}H_{qij}^{pij} \longrightarrow \varepsilon_q^p \delta_{pq}, \quad (2.32)$$

where ε_q^p is the eigenvalue of the Fock operator.

A practical way of solving this system of equations is to express each new orbital in the unknown Hatree-Fock basis, $|p'\rangle \equiv \phi_{p'}(\mathbf{r})$, denoted with primed labels, as a linear combination of the known single-particle basis states, $|p\rangle \equiv \phi_p(\mathbf{r})$, denoted without primed labels.

$$|p'\rangle = \sum_p \langle p | p' \rangle |p\rangle = \sum_p C_{p'}^p |p\rangle \quad (2.33)$$

Then the Fock matrix can be written in terms of the Hartree-Fock basis,

$$\begin{aligned} f_{q'}^{p'} &= {}^{(1)}H_{q'}^{p'} + \sum_{i'} {}^{(2)}H_{q'i'}^{p'i'} + \frac{1}{2} \sum_{i'j'} {}^{(3)}H_{q'i'j'}^{p'i'j'} \\ &= \sum_{pq} C_p^{p'*} {}^{(1)}H_q^p C_{q'}^q + \sum_{\substack{i' \\ prqs}} C_p^{p'*} C_r^{i'*} {}^{(2)}H_{qs}^{pr} C_{q'}^q C_{i'}^s + \frac{1}{2} \sum_{\substack{i'j' \\ prsqtu}} C_p^{p'*} C_r^{i'*} C_s^{j'*} {}^{(3)}H_{qtu}^{prs} C_{q'}^q C_{i'}^t C_{j'}^u. \end{aligned} \quad (2.34)$$

Defining the first-order density matrix γ_q^p as the product of expansion coefficients, summed over all shared hole states,

$$\gamma_q^p = \sum_{i'} C_{i'}^p C_q^{i'*}, \quad (2.35)$$

Eq. (2.33) is simplified to,

$$f_{q'}^{p'} = \sum_{pq} C_p^{p'*} \left[{}^{(1)}H_q^p + \sum_{rs} \gamma_s^r {}^{(2)}H_{qs}^{pr} + \frac{1}{2} \sum_{rstu} \gamma_t^r \gamma_u^s {}^{(3)}H_{qtu}^{prs} \right] C_{q'}^q \longrightarrow \varepsilon_{q'}^{p'} \delta_{p'q'}. \quad (2.36)$$

Therefore, the Hartree-Fock equations are ultimately expressed as an eigenvalue problem where the matrix to diagonalize is the Fock matrix in the form,

$$\hat{F}_q^p (\hat{C}) = {}^{(1)}H_q^p + \sum_{rs} \gamma_r^s {}^{(2)}H_{qs}^{pr} + \frac{1}{2} \sum_{rstu} \gamma_r^t \gamma_s^u {}^{(3)}H_{qtu}^{prs}, \quad (2.37)$$

and the matrix of coefficients, $\hat{C} = C_{p'}^p$, is the unitary operator that transforms the matrix to a diagonal form,

$$\sum_{pq} C_p^{p'*} \hat{F}_q^p (\hat{C}) C_{q'}^q = \varepsilon_{q'}^{p'} \delta_{p'q'} \quad (2.38)$$

The iterative nature of the solution comes from the dependence of the Fock matrix on the transformation coefficients. These Hartree-Fock equations are solved numerically by using an iterative algorithm where the Fock matrix is built using a known set of coefficients and diagonalized to obtain an updated set of coefficients. This process is repeated until the unitary set of coefficients is unchanged within a certain tolerance. For most calculations, using the identity matrix as an initial guess for the coefficients is sufficient. To improve the rate of convergence, techniques such as the direct inversion of the iterative subspace (DIIS) [91, 90] or Broyden's method [21] can be implemented. And, to avoid any oscillatory behavior around the solution, techniques such as the level-shifting method or *ad hoc* linear mixing can be implemented to dampen the large changes between iterations.

To make use of the HF solution as the reference state for post-HF calculations, the Hamiltonian matrix elements must be transformed to the new basis and the normal-ordered

version redefined to account for the additional reordering of one-particle correlations into the HF energy.

$$f_{q'}^{p'} = \varepsilon_{q'}^{p'} \delta_{p'q'} \quad (2.39)$$

$$V_{r's'}^{p'q'} = \sum_{pqrs} C_p^{p'*} C_q^{q'*} \left({}^{(2)}H_{rs}^{pq} + {}^{(3)}H_{rsu}^{pqt} \gamma_t^u \right) C_{r'}^r C_{s'}^s \quad (2.40)$$

$$\begin{aligned} E_0 &= \sum_{i'} {}^{(1)}H_{i'}^{i'} + \frac{1}{2} \sum_{i'j'} {}^{(2)}H_{i'j'}^{i'j'} + \frac{1}{6} \sum_{i'j'k'} {}^{(3)}H_{i'j'k'}^{i'j'k'} \\ &= \sum_{i'} \varepsilon_{i'}^{i'} - \frac{1}{2} \sum_{i'j'} V_{i'j'}^{i'j'} + \frac{1}{6} \sum_{i'j'k'} {}^{(3)}H_{i'j'k'}^{i'j'k'} \end{aligned} \quad (2.41)$$

Additionally, any operators that are constructed in the original basis must be transformed in a similar manner. For example, a one-body operator \hat{O} in the Hartree-Fock basis is,

$$\begin{aligned} \hat{O} &= \sum_{p'q'} O_{q'}^{p'} \left\{ \hat{a}_{p'}^\dagger \hat{a}_{q'} \right\} = \sum_{p'q'pq} C_p^{p'*} O_q^p C_{q'}^q \left\{ \hat{a}_{p'}^\dagger \hat{a}_{q'} \right\} \\ &\longrightarrow O_{q'}^{p'} = \sum_{pq} C_p^{p'*} O_q^p C_{q'}^q. \end{aligned} \quad (2.42)$$

Because the Hartree-Fock basis is diagonal in the one-body piece of the Hamiltonian, any terms that include off-diagonal elements automatically vanish, greatly simplifying any post-Hartree-Fock methods. From this point, any calculations will use the Hartree-Fock basis unless stated otherwise, and prime symbols will be omitted.

2.6 Configuration-Interaction

The most generic way to write a correlated wave function in a given basis is as a linear combination of all possible Slater determinants. In normal-ordered form, this expansion

can, in principle, consist of the $0p$ - $0h$ reference state and all possible Np - Nh excitations up to Ap - Ah excitations,

$$|\Psi_\nu\rangle = \sum_{\nu_i}^{\mathcal{N}} C_{\nu_i} |\Phi_{\nu_i}\rangle = C_0 |\Phi_0\rangle + \sum_{N=1}^A \left(\frac{1}{N!}\right)^2 \sum_{\substack{a_1 \dots a_N \\ i_1 \dots i_N}} C_{i_1 \dots i_N}^{a_1 \dots a_N} |\Phi_{i_1 \dots i_N}^{a_1 \dots a_N}\rangle. \quad (2.43)$$

Using this form of the wave function in Eq. (2.43), the Schrödinger equation can be reformulated as a standard matrix eigenvalue problem,

$$\begin{aligned} \hat{H}_N |\Psi_\nu\rangle &= \Delta E_\nu |\Psi_\nu\rangle \quad \longrightarrow \quad \langle \Psi_\mu | \hat{H}_N | \Psi_\nu \rangle = \Delta E_\nu \langle \Psi_\mu | \Psi_\nu \rangle \\ &= \sum_{\mu_i \nu_i} C_{\mu_i}^* \langle \Phi_{\mu_i} | \hat{H}_N | \Phi_{\nu_i} \rangle C_{\nu_i} = \Delta E_\nu \sum_{\mu_i \nu_i} C_{\mu_i}^* C_{\nu_i} \delta_{\mu_i \nu_i} \\ &\longrightarrow \mathbf{C}_\mu^T \left(\langle \Phi_{\mu_i} | \hat{H}_N | \Phi_{\nu_i} \rangle - \Delta E_\nu \mathbf{I} \right) \mathbf{C}_\nu = 0. \end{aligned} \quad (2.44)$$

In this case, the matrix elements are Hamiltonian terms that connect two Slater determinants, and the eigenvectors are the ground and excited states in the form of Eq. (2.43). The matrix elements can be found with the help of the Slater-Condon rules [100, 33] which, because the Hamiltonian is restricted to one- and two-body terms, require that any terms connecting Slater determinants which differ by more than two single-particle states vanish. Also, because the one-body Hamiltonian is diagonal in the Hatree-Fock basis, it only contributes to diagonal elements the CI matrix. Some examples of these matrix elements

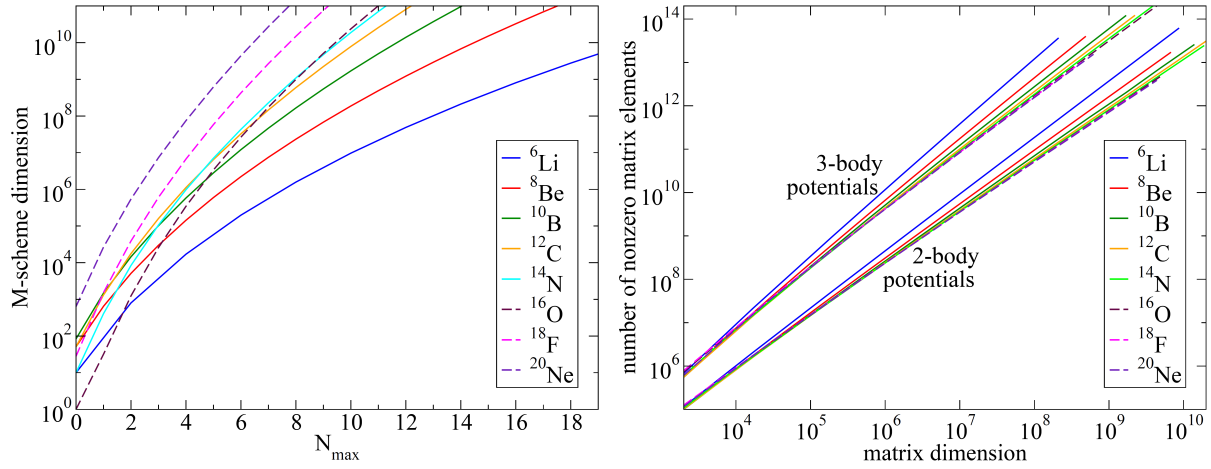


Figure 2.3: Scaling of the matrix size and number of non-zero matrix elements for nuclear CI calculations of light nuclei. Even for modest N_{\max} , the memory requirements approach the limit of petascale supercomputers (10^{10}). Figure taken from [96].

are,

$$\langle \Phi_i^a | \hat{H} | \Phi_i^a \rangle = \varepsilon_a - \varepsilon_i - V_{ia}^{ia} \quad (2.45)$$

$$\langle \Phi_{ij}^{ab} | \hat{H} | \Phi_{ij}^{cd} \rangle = V_{cd}^{ab} \quad (2.46)$$

$$\langle \Phi_{ijk}^{abc} | \hat{H} | \Phi_{ijl}^{abd} \rangle = -V_{kd}^{lc} \quad (2.47)$$

Because the configuration-interaction method exhaustively captures all the correlations of a many-body system, it is considered an “exact” method within a certain model space and becomes truly exact as the number of single-particle states is increased to infinity. However, there is a price to pay for this exactness. The number of Slater determinants, \mathcal{N} , in model space scales factorially according to Eq. (2.5) and the configuration-interaction matrix scales as \mathcal{N}^2 . For sufficiently-sized model spaces, the memory required for this matrix quickly becomes unmanigable even for the largest supercomputers.

However, for a reference state that is a good approximation to the true ground state, few-body excitations generally dominate the wave functions for low-lying states [98]. This

can be exploited by truncating the expansion in Eq. (2.43). Owing to the two-body nature of the interaction, the lowest appropriate truncation is also at the two-body level, known as configuration interaction with singles and doubles (CISD),

$$|\Psi_\nu\rangle = C_0|\Phi_0\rangle + \sum_{ai} C_i^a |\Phi_i^a\rangle + \frac{1}{4} \sum_{abij} C_{ij}^{ab} |\Phi_{ij}^{ab}\rangle. \quad (2.48)$$

This is a very straightforward and tractable way to approximate the many-body Schrödinger equation, and it can be systematically improved by adding more excitations such as triples (CISDT) or triples and quadruples (CISDTQ). But the drawback to this simplicity is that any truncated CI method is not size-extensive such that any extensive property of a system, like the energy, would scale with the size of the system. A desirable many-body method will be both systematically improvable and size-extensive while maintaining computational feasibility.

2.7 Many-Body Perturbation Theory

One many-body method that is both size-extensive and systematically improvable treats particle-particle interactions as a perturbation to the mean-field potential and is known as many-body perturbation theory (MBPT) [81, 62, 63, 97]. The Hamiltonian is partitioned into a diagonal piece and the interaction piece,

$$\begin{aligned} \hat{H} &= \hat{H}_0 + \hat{V}, \quad \text{with} \\ \hat{H}_0 &= E_0 + \sum_p f_p^p \left\{ \hat{a}_p^\dagger \hat{a}_p \right\} \quad \text{and} \\ \hat{V} &= \frac{1}{4} \sum_{pqrs} V_{rs}^{pq} \left\{ \hat{a}_p^\dagger \hat{a}_q^\dagger \hat{a}_s \hat{a}_r \right\} \end{aligned} \quad (2.49)$$

When not in the Hartree-Fock basis, the interaction piece has the additional off-diagonal Fock term, $\sum_{p \neq q} f_q^p \{ \hat{a}_p^\dagger \hat{a}_q \}$. This means that the reference state is an eigenstate of the zero-order piece of the Hamiltonian,

$$\hat{H}_0 |\Phi_0\rangle = \left(E_0 + \sum_i f_i^i \{ \hat{a}_i^\dagger \hat{a}_i \} \right) |\Phi_0\rangle = \left(E_0 + \sum_i \varepsilon_i \right) |\Phi_0\rangle = E_0^{(0)} |\Phi_0\rangle \quad (2.50)$$

.

Using *intermediate normalization*, which sets $\langle \Phi_0 | \Psi \rangle = 1$, the Schrödinger equation, Eq. (2.1) for the ground state, becomes,

$$\begin{aligned} \langle \Phi_0 | (\hat{H}_0 + \hat{V}) | \Psi \rangle &= \langle \Phi_0 | \hat{H}_0 | \Psi \rangle + \langle \Phi_0 | \hat{V} | \Psi \rangle = E \langle \Phi_0 | \Psi \rangle \\ &= E^{(0)} \langle \Phi_0 | \Psi \rangle + \langle \Phi_0 | \hat{V} | \Psi \rangle = E^{(0)} + \langle \Phi_0 | \hat{V} | \Psi \rangle = E. \end{aligned} \quad (2.51)$$

Next, the projection operators \hat{P} and \hat{Q} can be introduced,

$$\hat{P} = |\Phi_0\rangle \langle \Phi_0|, \quad (2.52)$$

$$\hat{Q} = \sum_{n \neq 0} |\Phi_n\rangle \langle \Phi_n| = 1 - |\Phi_0\rangle \langle \Phi_0|. \quad (2.53)$$

The \hat{P} operator isolates the reference-state component of any Slater determinant while the \hat{Q} operator isolates all components *except* the reference-state component out of any Slater determinant. Both these operators are idempotent, which means that $\hat{P}^2 = \hat{P}$ and $\hat{Q}^2 = \hat{Q}$, and because of intermediate normalization, the correlated wave function can be written as $|\Psi\rangle = (\hat{P} + \hat{Q})|\Psi\rangle = |\Phi\rangle + \hat{Q}|\Psi\rangle$. Also, both operators commute with the unperturbed part of the Hamiltonian, $\hat{H}_0 \hat{P} = \hat{P} \hat{H}_0$ and $\hat{H}_0 \hat{Q} = \hat{Q} \hat{H}_0$. These identities can be applied to an alternate version of the Schrödinger equation which defines a particular version of perturba-

tion theory known as Raleigh-Schrödinger perturbation theory (RSPT). In this version, the zeroth-order energy $E^{(0)}$ is added to both sides of the Schrödinger equation. Acting with \hat{Q} and rearranging terms gives,

$$\begin{aligned}\hat{Q}(E^{(0)} - \hat{H}_0)|\Psi\rangle &= \hat{Q}(E^{(0)} + \hat{V} - E)|\Psi\rangle \\ \hat{Q}(E^{(0)} - \hat{H}_0)\hat{Q}|\Psi\rangle &= \hat{Q}(\hat{V} - \Delta E_0)|\Psi\rangle,\end{aligned}\tag{2.54}$$

where $\Delta E_0 \equiv E - E^{(0)} = \langle \Phi_0 | \hat{V} | \Psi \rangle$. The operator $\hat{Q}(E^{(0)} - \hat{H}_0)\hat{Q}$ is invertible because $(E^{(0)} - \hat{H}_0)^{-1}$ is never singular in Q -space. Therefore, the operator $\hat{R}_0 = \hat{Q}(E^{(0)} - \hat{H}_0)^{-1}\hat{Q}$, known as the *resolvent*, can be applied to both sides to result in the generating equation for RSPT,

$$\begin{aligned}\hat{Q}(E^{(0)} - \hat{H}_0)^{-1}(E^{(0)} - \hat{H}_0)\hat{Q}|\Psi\rangle &= \hat{Q}(E^{(0)} - \hat{H}_0)^{-1}\hat{Q}(\hat{V} - \Delta E_0)|\Psi\rangle \\ \hat{Q}|\Psi\rangle &= \hat{R}_0(\hat{V} - \Delta E_0)|\Psi\rangle \\ |\Psi\rangle &= |\Phi\rangle + \hat{R}_0(\hat{V} - \Delta E_0)|\Psi\rangle\end{aligned}\tag{2.55}$$

Because the single-particle states are eigenfunctions of the zeroth-order Hamiltonian, they are also eigenfunctions of the resolvent. The resulting eigenvalues are known as *energy denominators*,

$$\begin{aligned}\hat{R}_0|\Phi_{i_1 \dots i_N}^{a_1 \dots a_N}\rangle &= \frac{1}{\varepsilon_{i_1 \dots i_N}^{a_1 \dots a_N}}|\Phi_{i_1 \dots i_N}^{a_1 \dots a_N}\rangle, \text{ where} \\ \varepsilon_{i_1 \dots i_N}^{a_1 \dots a_N} &= \varepsilon_{i_1} + \dots + \varepsilon_{i_N} - \varepsilon_{a_1} - \dots - \varepsilon_{a_N}\end{aligned}\tag{2.56}$$

Equation (2.7) can be iterated infinitely to give the solution for the fully correlated wave

function which can, in turn, be used to solve for the energy with Eq. (2.51),

$$|\Psi\rangle = \sum_{n=0}^{\infty} \left[\hat{R}_0 (\hat{V} - \Delta E_0) \right]^n |\Phi_0\rangle, \quad (2.57)$$

$$\Delta E_0 = \langle \Phi_0 | \hat{V} | \Psi \rangle = \sum_{n=0}^{\infty} \langle \Phi_0 | \hat{V} \left[\hat{R}_0 (\hat{V} - \Delta E_0) \right]^n |\Phi_0\rangle \quad (2.58)$$

The immediate problem with this equation is that the right-hand side of the equations contain the target energy difference ΔE_0 for which these equations are meant to solve. This can be remedied by expanding the right-hand sides and rearranging terms. Using the fact that $\hat{R}_0 \Delta E_0 |\Phi_0\rangle = \Delta E_0 \hat{R}_0 |\Phi_0\rangle = 0$, the first-order energy $E^{(1)} = \langle \Phi_0 | \hat{V} | \Phi_0 \rangle$, and the shifted term $\tilde{V} \equiv \hat{V} - E^{(1)}$, these simplify to,

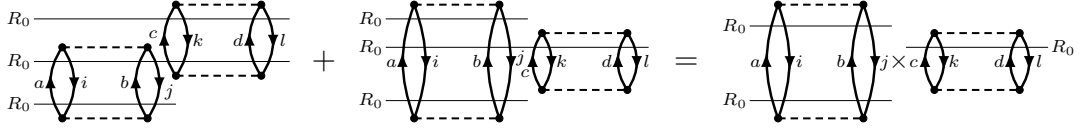
$$\begin{aligned} |\Psi\rangle - |\Phi_0\rangle &= \hat{R}_0 \hat{V} |\Phi_0\rangle + \hat{R}_0 \tilde{V} \hat{R}_0 \hat{V} |\Phi_0\rangle \\ &+ \hat{R}_0 \tilde{V} \hat{R}_0 \tilde{V} \hat{R}_0 \hat{V} |\Phi_0\rangle - \langle \Phi_0 | \hat{V} \hat{R}_0 \hat{V} | \Phi_0 \rangle \hat{R}_0^2 \hat{V} |\Phi_0\rangle + \dots \end{aligned} \quad (2.59)$$

$$\begin{aligned} \Delta E_0 &= \langle \Phi_0 | \hat{V} | \Phi_0 \rangle + \langle \Phi_0 | \hat{V} \hat{R}_0 \hat{V} | \Phi_0 \rangle + \langle \Phi_0 | \hat{V} \hat{R}_0 \tilde{V} \hat{R}_0 \hat{V} | \Phi_0 \rangle \\ &+ \langle \Phi_0 | \hat{V} \hat{R}_0 \tilde{V} \hat{R}_0 \tilde{V} \hat{R}_0 \hat{V} | \Phi_0 \rangle - \langle \Phi_0 | \hat{V} \hat{R}_0 \hat{V} | \Phi_0 \rangle \langle \Phi_0 | \hat{V} \hat{R}_0^2 \hat{V} | \Phi_0 \rangle + \dots \end{aligned} \quad (2.60)$$

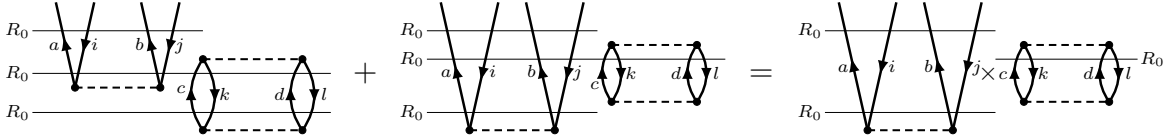
The order of each term can be easily identified by counting the numbers of times that \hat{V} or \tilde{V} appears. At the third order in the wave function and the fourth order in the energy, *renormalization* terms make their first appearance. These terms contain separated and closed factors in the form of lower-order energy terms, such as $\langle \Phi_0 | \hat{V} \hat{R}_0 \hat{V} | \Phi_0 \rangle \equiv E^{(2)}$. Terms that do not contain normalization factors are known as *principle* terms.

2.7.1 Factorization Theorem

A powerful application of diagrammatic techniques known as the *factorization theorem* [63, 45, 18] can immediately be used to simplify these expansions. By factoring sums of *unlinked* diagrams, where two or more parts of a diagram are closed and separated, from the principle terms, it can be shown that they exactly cancel with the renormalization terms at each order.



$$\begin{aligned}
& \frac{1}{16} \sum_{abcd} \frac{V_{ab}^{ij} V_{ij}^{ab} V_{cd}^{kl} V_{kl}^{cd}}{\varepsilon_{ij}^{ab} \varepsilon_{ijkl}^{abcd} \varepsilon_{kl}^{cd}} + \frac{1}{16} \sum_{abcd} \frac{V_{ab}^{ij} V_{ij}^{ab} V_{cd}^{kl} V_{kl}^{cd}}{\varepsilon_{ij}^{ab} \varepsilon_{ijkl}^{abcd} \varepsilon_{ij}^{ab}} = \frac{1}{16} \sum_{abcd} V_{ab}^{ij} V_{ij}^{ab} V_{cd}^{kl} V_{kl}^{cd} \frac{\varepsilon_{ij}^{ab} + \varepsilon_{kl}^{cd}}{(\varepsilon_{ij}^{ab})^2 \varepsilon_{ijkl}^{abcd} \varepsilon_{kl}^{cd}} \\
& = \frac{1}{4} \sum_{abij} \frac{V_{ab}^{ij} V_{ij}^{ab}}{(\varepsilon_{ij}^{ab})^2} \cdot \frac{1}{4} \sum_{cdkl} \frac{V_{cd}^{kl} V_{kl}^{cd}}{\varepsilon_{kl}^{cd}} = \langle \Psi_n^{(1)} | \Psi_n^{(1)} \rangle E_n^{(2)} \quad (2.61)
\end{aligned}$$



$$\begin{aligned}
& \frac{1}{16} \sum_{abcd} \frac{V_{ij}^{ab} V_{cd}^{kl} V_{kl}^{cd}}{\varepsilon_{kl}^{cd} \varepsilon_{ijkl}^{abcd} \varepsilon_{ij}^{ab}} |\Phi_{ij}^{ab}\rangle + \frac{1}{16} \sum_{abcd} \frac{V_{ij}^{ab} V_{cd}^{kl} V_{kl}^{cd}}{\varepsilon_{ij}^{ab} \varepsilon_{ijkl}^{abcd} \varepsilon_{ij}^{ab}} |\Phi_{ij}^{ab}\rangle = \frac{1}{16} \sum_{abcd} V_{ij}^{ab} V_{cd}^{kl} V_{kl}^{cd} \frac{\varepsilon_{ij}^{ab} + \varepsilon_{kl}^{cd}}{(\varepsilon_{ij}^{ab})^2 \varepsilon_{ijkl}^{abcd} \varepsilon_{kl}^{cd}} |\Phi_{ij}^{ab}\rangle \\
& = \frac{1}{4} \sum_{abij} \frac{V_{ij}^{ab}}{(\varepsilon_{ij}^{ab})^2} |\Phi_{ij}^{ab}\rangle \cdot \frac{1}{4} \sum_{cdkl} \frac{V_{cd}^{kl} V_{kl}^{cd}}{\varepsilon_{kl}^{cd}} = \frac{|\Psi_n^{(1)}\rangle}{\varepsilon_n} E_n^{(2)} \quad (2.62)
\end{aligned}$$

The factorization theorem is also valid with off-diagonal Fock terms and applies to the MBPT expansions of both the wave function and energy. Therefore, these can be written in

terms of *linked diagrams* only,

$$|\Psi\rangle = \sum_{n=0}^{\infty} \left[\hat{R}_0 (\hat{V} - \Delta E_0) \right]^n |\Phi_0\rangle_{\text{L}}, \quad (2.63)$$

$$\Delta E_0 = \sum_{n=0}^{\infty} \langle \Phi_0 | \hat{V} \left[\hat{R}_0 (\hat{V} - \Delta E_0) \right]^n |\Phi_0\rangle_{\text{L}}, \quad (2.64)$$

where “L” denotes that no diagrams with closed, disconnected pieces should be included. This result not only simplifies the MBPT expressions, but it guarantees the size-extensivity of the MBPT wave function at each order [97]. Also, it is a useful step towards coupled-cluster theory which reorganizes the connected diagrams from MBPT such that certain classes can be summed to infinite order, see section 3.2.

Chapter 3

Coupled-Cluster Theory

Coupled-cluster theory is a powerful method for approximating solutions to the many-body Schrödinger equation. Because of its effectiveness and economical scaling it has been a staple of many-body quantum mechanics for decades. This chapter details various aspects of the coupled-cluster approach and presents ground-state results for multiple systems. First, the CC wave operator and the corresponding effective Hamiltonian will be introduced and used to derive the CC equations. Then, results from MBPT are used to illuminate the underlying many-body physics of the CC wave function. After the mathematical foundations of coupled cluster theory are outlined, specific implementation details are discussed and demonstrated by focusing on two simple examples. Finally, the nuclear many-body problem is formally introduced, along with a brief description of the nuclear interactions used in this work, and selected results are shown.

3.1 Exponential Ansatz

Coupled cluster theory is based on expressing the A -particle correlated wave function $|\Psi\rangle$ using the exponential ansatz,

$$|\Psi\rangle = e^{\hat{T}} |\Phi_0\rangle. \quad (3.1)$$

The cluster operator $\hat{T} \equiv \hat{T}_1 + \hat{T}_2 + \cdots + \hat{T}_A$, is composed of k -particle k -hole excitation operators, \hat{T}_k , which have the form,

$$\begin{aligned}
\hat{T}_1 &\equiv \sum_{ai} t_i^a \left\{ \hat{a}_a^\dagger \hat{a}_i \right\}, \\
\hat{T}_2 &\equiv \frac{1}{4} \sum_{abij} t_{ij}^{ab} \left\{ \hat{a}_a^\dagger \hat{a}_b^\dagger \hat{a}_j \hat{a}_i \right\}, \\
&\vdots \\
\hat{T}_k &\equiv \left(\frac{1}{k!} \right)^2 \sum_{\substack{a_1 \dots a_k \\ i_1 \dots i_k}} t_{i_1 \dots i_k}^{a_1 \dots a_k} \left\{ \hat{a}_{a_1}^\dagger \cdots \hat{a}_{a_k}^\dagger \hat{a}_{i_k} \cdots \hat{a}_{i_1} \right\}.
\end{aligned} \tag{3.2}$$

where the unknown matrix elements, $t_{i_1 \dots i_k}^{a_1 \dots a_k}$, are known as *cluster amplitudes* [97].

Using the CC ansatz, the Schrödinger equation can be rewritten by left-multiplying with $\langle \Phi_0 | e^{-\hat{T}}$ as,

$$\begin{aligned}
\hat{H} e^{\hat{T}} |\Phi_0\rangle &= E e^{\hat{T}} |\Phi_0\rangle \\
\longrightarrow \langle \Phi_0 | \bar{H} | \Phi_0 \rangle &= E,
\end{aligned} \tag{3.3}$$

where the *coupled cluster effective Hamiltonian* is defined as,

$$\bar{H} \equiv e^{-\hat{T}} \hat{H} e^{\hat{T}}, \tag{3.4}$$

in which the wave operator, $e^{\hat{T}}$, acts as a similarity transform on the Hamiltonian.

An important characteristic of the effective Hamiltonian, \bar{H} , is that because the cluster operator, which contains no de-excitations, is not Hermitian, the exponential wave operator cannot be unitary, and thus \bar{H} is not Hermitian. This initially seems like an explicit con-

tradiction to any standard quantum mechanics formulation where observables are associated with the real eigenvalues of Hermitian matrices. Technically, the existence and reality of the CC solution is only guaranteed when the full cluster operator is used $\hat{T} = \hat{T}_1 + \cdots + \hat{T}_A$, see [125, 80]. However, while the non-Hermiticity does require some special considerations which will be discussed, this fundamental problem does not materialize in this work.

The effective Hamiltonian in Eq. (3.4) can be rewritten with commutators $([\hat{A}, \hat{B}] = \hat{A}\hat{B} - \hat{B}\hat{A})$ according to the Baker–Campbell–Hausdorff expansion as,

$$\bar{H} = \hat{H} + [\hat{H}, \hat{T}] + \frac{1}{2!}[[\hat{H}, \hat{T}], \hat{T}] + \frac{1}{3!}[[[\hat{H}, \hat{T}], \hat{T}], \hat{T}] + \frac{1}{4!}[[[[\hat{H}, \hat{T}], \hat{T}], \hat{T}], \hat{T}] + \cdots,$$

which terminates at four-nested commutators when using a two-body interaction. This commutator expression ensures that CC is size-extensive and contains only connected terms. In addition, because \hat{T} is an excitation operator, terms of the form $\hat{T}\hat{H}$ are necessarily disconnected and thus vanish [97]. Therefore the CC effective Hamiltonian can be further reduced to

$$\bar{H} = \left(\hat{H} e^{\hat{T}} \right)_c, \quad (3.5)$$

where the subscript “c” indicates that only connected terms are used.

3.1.1 The Coupled Cluster Equations

In practice, the cluster operator \hat{T} must be truncated for calculations to be computationally feasible. In this work, we use only single and double excitations where applicable,

$$\hat{T} = \hat{T}_1 + \hat{T}_2.$$

This is known as coupled cluster with singles and doubles (CCSD), with an asymptotic computational cost that scales like $\mathcal{O}(n_p^4 n_h^2)$, where n_h is the number of hole states and n_p is the number of particle states. This truncation has been successfully applied to many problems in quantum chemistry [7] and nuclear physics [70, 53].

The unknown cluster amplitudes in CCSD, t_i^a and t_{ij}^{ab} , can be calculated by left-multiplying Eq. (3.1) with $\langle \Phi_i^a | e^{-\hat{T}}$ and with $\langle \Phi_{ij}^{ab} | e^{-\hat{T}}$, respectively,

$$\begin{aligned}\langle \Phi_i^a | \bar{H} | \Phi_0 \rangle &= 0, \\ \langle \Phi_{ij}^{ab} | \bar{H} | \Phi_0 \rangle &= 0.\end{aligned}\tag{3.6}$$

After the Fock matrix has been diagonalized, the diagonal components of Eq. (3.6) can be separated and, after expanding the exponent in Eq. (3.5), the non-vanishing terms of the CCSD amplitude equations become,

$$\begin{aligned}\langle \Phi_i^a | \left[\hat{H}_2 \left(\hat{T}_1 + \hat{T}_2 + \hat{T}_1 \hat{T}_2 + \frac{1}{2!} \hat{T}_1^2 + \frac{1}{3!} \hat{T}_1^3 \right) \right] | \Phi_0 \rangle &= \varepsilon_i^a t_i^a \\ \langle \Phi_{ij}^{ab} | \left[\hat{H}_2 \left(1 + \hat{T}_1 + \hat{T}_2 + \frac{1}{2} \hat{T}_1^2 + \hat{T}_1 \hat{T}_2 + \frac{1}{2!} \hat{T}_2^2 + \frac{1}{3!} \hat{T}_1^3 + \frac{1}{2!} \hat{T}_1^2 \hat{T}_2 + \frac{1}{4!} \hat{T}_1^4 \right) \right] | \Phi_0 \rangle &= \varepsilon_{ij}^{ab} t_{ij}^{ab}\end{aligned}\tag{3.7}$$

where ε are equivalent to the MBPT energy denominators from Eq. (2.7).

These non-linear equations are solved using an iterative procedure where the cluster amplitudes on the right-hand side of Eq. (3.6) and Eq. (3.7) are updated by calculating the terms on the left-hand side until a fixed point is reached. Like the HF iterative procedure, employing convergence acceleration techniques can reduce the number of CC iterations required. Detailed techniques for solving these equations are discussed in section 3.4.

3.2 Linked-Cluster Theorem and MBPT

The exponential ansatz in Eq. (3.1) and the cluster amplitudes in Eq. (3.1) are not just useful mathematical constructs for solving the many-body problem. They represent physical many-body dynamics and can be derived from the results of many-body perturbation theory, see section 2.7. The *linked-cluster theorem* [63, 45, 18] states that the sum of all time orderings of a disconnected diagram is equal to the product of the two subdiagrams. Using the results and techniques from the factorization theorem, 2.7.1, the linked-cluster theorem can be used to factorize specific MBPT terms such that they can be analytically summed to infinite order. This infinite summation is the main principle behind coupled cluster theory and can be shown to lead naturally to the exponential ansatz.

The first step in deriving the exponential ansatz is to group all the linked MBPT diagrams of Eq. (2.63) into classes according to their number of disconnected pieces. The first class, where all the terms are connected, can be defined as the cluster excitation operator \hat{T} . The connected terms can then be characterized by their excitation type such that \hat{T}_k corresponds to kp - kh excitations. The \hat{T}_1 , \hat{T}_2 , and \hat{T}_3 cluster amplitudes are shown in terms of the connected MBPT diagrams (only first-order $\hat{T}^{(1)}$ and second-order $\hat{T}^{(2)}$ terms are shown and resolvent lines are removed for clarity).

$$\begin{aligned}
 \hat{T}_1 |\Phi_0\rangle \equiv \underline{\text{V}} &= \left(\hat{T}_1^{(1)} + \hat{T}_1^{(2)} + \dots \right) |\Phi_0\rangle = \text{V} \cdots \times + \text{V} \text{---} \text{loop} \cdots \times + \text{loop} \text{---} \text{V} \cdots \times \\
 &+ \text{V} \text{---} \text{V} \cdots \times + \text{V} \text{---} \text{V} \text{---} \text{V} \cdots \times + \text{loop} \text{---} \text{V} \cdots \times + \text{loop} \text{---} \text{V} \text{---} \text{V} \cdots \times + \dots
 \end{aligned} \tag{3.8}$$

$$\begin{aligned}
\hat{T}_2 |\Phi_0\rangle \equiv \text{Diagram 1} &= (\hat{T}_2^{(1)} + \hat{T}_2^{(2)} + \dots) |\Phi_0\rangle = \text{Diagram 2} + \text{Diagram 3} + \text{Diagram 4} \\
&+ \text{Diagram 5} + \text{Diagram 6} + \text{Diagram 7} + \text{Diagram 8} + \dots
\end{aligned} \tag{3.9}$$

$$\begin{aligned}
\hat{T}_3 |\Phi_0\rangle \equiv \text{Diagram 9} &= (\hat{T}_3^{(2)} + \dots) |\Phi_0\rangle = \text{Diagram 10} + \text{Diagram 11} + \dots
\end{aligned} \tag{3.10}$$

So far, this is merely a redefinition of the connected class of MBPT diagrams up to all orders and is not particularly useful. But the disconnected diagrams, neglected up to this point, can be recombined using the factorization theorem to provide a powerful simplification. As an example, the remaining disconnected first- and second-order diagrams can be written as the product of connected diagrams,

$$\begin{aligned}
\text{Diagram 12} &= \frac{1}{2} \left(\text{Diagram 13} + \text{Diagram 14} \right) = \frac{1}{2} \left(\text{Diagram 15} \right)^2 \\
\sum_{abij} \frac{f_i^a f_j^b}{\varepsilon_{ij}^{ab} \varepsilon_i^a} |\Phi_{ij}^{ab}\rangle &= \frac{1}{2} \sum_{abij} \frac{f_i^a f_j^b}{\varepsilon_{ij}^{ab} \varepsilon_i^a} |\Phi_{ij}^{ab}\rangle + \frac{1}{2} \sum_{abij} \frac{f_i^a f_j^b}{\varepsilon_{ij}^{ab} \varepsilon_j^b} |\Phi_{ij}^{ab}\rangle = \frac{1}{2} \sum_{abij} f_i^a f_j^b \frac{\varepsilon_j^b + \varepsilon_i^a}{\varepsilon_{ij}^{ab} \varepsilon_i^a \varepsilon_j^b} |\Phi_{ij}^{ab}\rangle \\
&= \frac{1}{2} \left(\sum_{ai} \frac{f_i^a}{\varepsilon_i^a} |\Phi_i^a\rangle \right) \left(\sum_{bj} \frac{f_j^b}{\varepsilon_j^b} |\Phi_j^b\rangle \right) = \frac{1}{2} \left(\hat{T}_1^{(1)} \right)^2
\end{aligned} \tag{3.11}$$

$$\begin{aligned}
\text{Diagram 1} &= \frac{1}{2} \left(\text{Diagram 2} + \text{Diagram 3} \right) \\
&= \frac{1}{2} \left(\text{Diagram 4} \right)^2
\end{aligned}$$

$$\begin{aligned}
\frac{1}{16} \sum_{\substack{abcd \\ ijkl}} \frac{V_{ij}^{ab} V_{kl}^{cd}}{\varepsilon_{ijkl} \varepsilon_{ij}^{ab}} |\Phi_{ijkl}^{abcd}\rangle &= \frac{1}{32} \sum_{\substack{abcd \\ ijkl}} \frac{V_{ij}^{ab} V_{kl}^{cd}}{\varepsilon_{ijkl} \varepsilon_{ij}^{ab}} |\Phi_{ijkl}^{abcd}\rangle + \frac{1}{32} \sum_{\substack{abcd \\ ijkl}} \frac{V_{ij}^{ab} V_{kl}^{cd}}{\varepsilon_{ijkl} \varepsilon_{kl}^{cd}} |\Phi_{ijkl}^{abcd}\rangle \\
&= \frac{1}{32} \sum_{\substack{abcd \\ ijkl}} V_{ij}^{ab} V_{kl}^{cd} \frac{\varepsilon_{kl}^{cd} + \varepsilon_{ij}^{ab}}{\varepsilon_{ijkl} \varepsilon_{ij}^{ab} \varepsilon_{kl}^{cd}} |\Phi_{ijkl}^{abcd}\rangle \\
&= \frac{1}{2} \left(\frac{1}{4} \sum_{abij} \frac{V_{ij}^{ab}}{\varepsilon_{ij}^{ab}} |\Phi_{ij}^{ab}\rangle \right) \left(\frac{1}{4} \sum_{cdkl} \frac{V_{kl}^{cd}}{\varepsilon_{kl}^{cd}} |\Phi_{kl}^{cd}\rangle \right) = \frac{1}{2} \left(\hat{T}_2^{(1)} \right)^2 \quad (3.12)
\end{aligned}$$

$$\begin{aligned}
\text{Diagram 5} + \text{Diagram 6} &= \text{Diagram 7} \\
\frac{1}{4} \sum_{\substack{abc \\ ijk}} \frac{V_{ij}^{ab} f_k^c}{\varepsilon_{ijk} \varepsilon_{ij}^{ab}} |\Phi_{ijk}^{abc}\rangle + \frac{1}{4} \sum_{\substack{abc \\ ijk}} \frac{V_{ij}^{ab} f_k^c}{\varepsilon_{ijk} \varepsilon_k^c} |\Phi_{ijk}^{abc}\rangle &= \frac{1}{4} \sum_{\substack{abcd \\ ijkl}} V_{ij}^{ab} f_k^c \frac{\varepsilon_k^c + \varepsilon_{ij}^{ab}}{\varepsilon_{ijk} \varepsilon_{ij}^{ab} \varepsilon_k^c} |\Phi_{ijk}^{abc}\rangle \\
&= \left(\sum_{ck} \frac{f_k^c}{\varepsilon_k^c} |\Phi_k^c\rangle \right) \left(\frac{1}{4} \sum_{abij} \frac{V_{ij}^{ab}}{\varepsilon_{ij}^{ab}} |\Phi_{ij}^{ab}\rangle \right) = \hat{T}_1^{(1)} \hat{T}_2^{(1)} \quad (3.13)
\end{aligned}$$

Adding these factorized contributions gives $\frac{1}{2} \left(\hat{T}_1^{(1)} \right)^2 + \hat{T}_1^{(1)} \hat{T}_2^{(1)} + \frac{1}{2} \left(\hat{T}_2^{(1)} \right)^2 = \frac{1}{2} \left(\hat{T}_1^{(1)} + \hat{T}_2^{(1)} \right)^2$.

Repeating this procedure for all diagrams with two disconnected parts (L = 2) adds similar terms of all orders. The final contribution from this class of diagrams is,

$$\sum_{n=0}^{\infty} \left[\hat{R}_0 (\hat{V} - \Delta E_0) \right]^n |\Phi_0\rangle_{L=2} = \frac{1}{2} \hat{T}^2. \quad (3.14)$$

A similar form results from any class of diagrams with k disconnected pieces,

$$\sum_{n=0}^{\infty} \left[\hat{R}_0 (\hat{V} - \Delta E_0) \right]^n |\Phi_0\rangle_{L=k} = \frac{1}{k!} \hat{T}^k. \quad (3.15)$$

Therefore, summing over all classes of diagrams gives the final result that justifies the exponential ansatz,

$$|\Psi\rangle = \sum_{k=0}^{\infty} \sum_{n=0}^{\infty} \left[\hat{R}_0 (\hat{V} - \Delta E_0) \right]^n |\Phi_0\rangle_{L=k} = \sum_{k=0}^{\infty} \frac{1}{k!} \hat{T}^k |\Phi_0\rangle = e^{\hat{T}} |\Phi_0\rangle. \quad (3.16)$$

This equation shows the true strength and elegance of coupled cluster theory. By an ingenious reorganization and factorization of certain MBPT diagrams, the exponential ansatz captures the contribution of these excitations to infinite order. A more comprehensive derivation of the linked-cluster theorem can be found in [97].

3.3 Example: Pairing Model

It's beneficial to illustrate a simplified example of coupled cluster theory. For this purpose, we turn our attention to the simple pairing model. This system uses a model space of N shells, each with two opposite spin orbitals.

With a closed-shell reference state, the Hamiltonian is restricted to interact only between unbroken pairs, which can be written as,

$$\begin{aligned} {}^{(1)}\hat{H} &= \delta \sum_p^N (p-1) \left[\hat{a}_{p+}^\dagger \hat{a}_{p+} + \hat{a}_{p-}^\dagger \hat{a}_{p-} \right], \quad \text{and} \\ {}^{(2)}\hat{H} &= -\frac{g}{2} \sum_{pq}^N \hat{a}_{p+}^\dagger \hat{a}_{p-}^\dagger \hat{a}_{q-} \hat{a}_{q+}, \end{aligned} \quad (3.17)$$

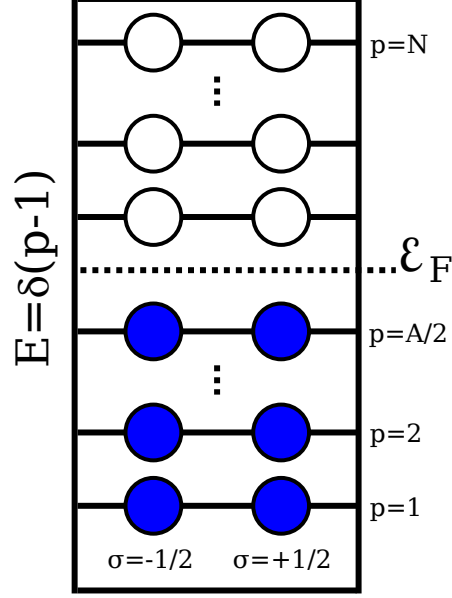


Figure 3.1: Schematic representation of the pairing model space. The shells are equally spaced and doubly degenerate with one spin-up and one spin-down state.

where δ and g are free parameters and the \pm labels represent the spin-up and spin-down states, respectively.

As with all other coupled cluster calculations in this work, the first step is transforming the problem to the Hartree-Fock basis. In this case, the restriction to unbroken pairs means that the original single-particle states do not mix with states in other shells. In fact, the original basis is already an eigenbasis of the Fock operator, Eq. (2.32), so that all is left of the HF transformation is to redefine the single-particle energies to their corresponding Hartree-Fock energies while the two-body interaction is left unchanged,

$$\begin{aligned} \varepsilon_{pm_p} &= {}^{(1)}H_{pm_p}^{pm_p} + \sum_{im_i} {}^{(2)}H_{pm_p im_i}^{pm_p im_i} = \delta(p-1) - \frac{g}{2} \\ V_{rs}^{pq} &= {}^{(2)}H_{rs}^{pq} \end{aligned} \quad (3.18)$$

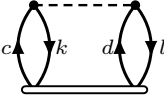
Again, because of the pairing restriction, only hole-state energies have to be redefined.

The next step in calculating the ground-state correlation energy is to solve the CCD equations in the Hartree-Fock basis. The system of equations comes from the terms of Eq. (3.7) that contain only the \hat{T}_2 operator, and are most easily derived with diagrammatic techniques, see [97].

$$\begin{aligned}
& \langle \Phi_{ij}^{ab} | (\hat{H} e^{\hat{T}_2})_C | \Phi_0 \rangle - \text{[diagram 1]} - \text{[diagram 2]} = \text{[diagram 3]} \\
& + \text{[diagram 4]} + \text{[diagram 5]} + \text{[diagram 6]} + \text{[diagram 7]} \\
& + \text{[diagram 8]} + \text{[diagram 9]} + \text{[diagram 10]} \\
& (\varepsilon_i + \varepsilon_j - \varepsilon_a - \varepsilon_b) t_{ij}^{ab} = V_{ij}^{ab} + \frac{1}{2} \sum_{kl} V_{ij}^{kl} t_{kl}^{ab} + \frac{1}{2} \sum_{cd} V_{cd}^{ab} t_{ij}^{cd} - \hat{P}(ij|ab) \sum_{kc} V_{ic}^{kb} t_{kj}^{ac} \\
& + \frac{1}{4} \sum_{klcd} V_{cd}^{kl} t_{kl}^{ab} t_{ij}^{cd} + \hat{P}(ab) \sum_{klcd} V_{cd}^{kl} t_{lj}^{ac} t_{ki}^{bd} - \hat{P}(ij) \frac{1}{2} \sum_{klcd} V_{cd}^{kl} t_{lj}^{ab} t_{ki}^{cd} - \hat{P}(ab) \frac{1}{2} \sum_{klcd} V_{cd}^{kl} t_{ij}^{db} t_{kl}^{ca}
\end{aligned} \tag{3.19}$$

The CCD equations are written in this particular form so that an initial guess for all the amplitudes t_{ij}^{ab} can be used to calculate the right-hand side of Eq. (3.3) and update the amplitudes on the left-hand side iteratively until the amplitudes do not change within a certain tolerance.

Lastly, the CCD correlation energy can be found with the \hat{T}_2 term of Eq. (3.1),

$$\Delta E_{\text{CCD}} = \langle \Phi_0 | (\hat{H} e^{\hat{T}_2})_C | \Phi_0 \rangle = \text{diagram} = \frac{1}{4} \sum_{klcd} V_{cd}^{kl} t_{kl}^{cd} \quad (3.20)$$


The correlation energies for a specific case, with $\delta = 1.0$, $N = 4$, and $A = 4$, were calculated for a number of different interaction strengths, g . The results are shown in Fig. 3.2 along with the MBPT correlation energies to third (MBPT3) and fourth (MBPT4) orders for comparison. The MBPT expressions for second and third order are,

$$\Delta E_{\text{MBPT2}} = \frac{1}{4} \sum_{ijab} \frac{V_{ab}^{ij} V_{ij}^{ab}}{\epsilon_{ij}^{ab}}, \quad (3.21)$$

$$\Delta E_{\text{MBPT3}} = \Delta E_{\text{MBPT2}} + \frac{1}{8} \sum_{ijabcd} \frac{V_{ab}^{ij} V_{cd}^{ab} V_{ij}^{cd}}{\epsilon_{ij}^{ab} \epsilon_{ij}^{cd}} + \frac{1}{8} \sum_{ijklab} \frac{V_{ab}^{ij} V_{ij}^{kl} V_{kl}^{ab}}{\epsilon_{ij}^{ab} \epsilon_{kl}^{ab}} - \sum_{ijkabc} \frac{V_{ab}^{ij} V_{ic}^{kb} V_{kj}^{ac}}{\epsilon_{ij}^{ab} \epsilon_{kj}^{ac}}. \quad (3.22)$$

The fourth-order expression contains 39 additional terms, so the expression for MBPT4 is omitted.

Also shown are the exact results from the CI method. With an example this small, it's possible to diagonalize, and even show explicitly, the full CI Hamiltonian matrix for an exact result. There are six possible Slater determinants with no broken pairs, one representing the reference state, four representing various $2p$ - $2h$ excitations, one representing a $4p$ - $4h$ excitation. The diagonal elements of the matrix include the single-particle energies of the constituent states, and the matrix elements between Slater determinants with no overlap

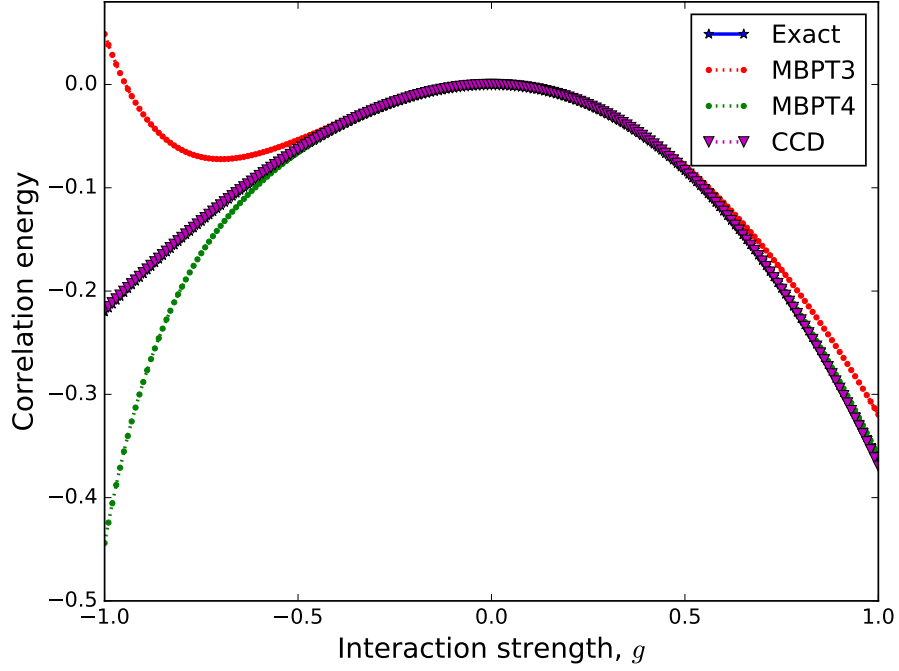


Figure 3.2: Correlation energy for the pairing model with exact diagonalization, CCD, and perturbation theory to third (MBPT3) and fourth order (MBPT4) for a range of interaction values, g .

vanish in accordance with the Slater-Condon rules, see Eq. (2.45) and [100, 33].

$$H = \begin{bmatrix} 2\delta - g & -g/2 & -g/2 & -g/2 & -g/2 & 0 \\ -g/2 & 4\delta - g & -g/2 & -g/2 & -0 & -g/2 \\ -g/2 & -g/2 & 6\delta - g & 0 & -g/2 & -g/2 \\ -g/2 & -g/2 & 0 & 6\delta - g & -g/2 & -g/2 \\ -g/2 & 0 & -g/2 & -g/2 & 8\delta - g & -g/2 \\ 0 & -g/2 & -g/2 & -g/2 & -g/2 & 10\delta - g \end{bmatrix} \quad (3.23)$$

As methods to obtain the ground-state correlation energy, both CI and CC decouple, to some degree, the reference state and excitations from it. This decoupling has the effect of shuffling correlations into the reference state and suppressing matrix elements connected to

it. Full decoupling between the reference state and all other Slater determinants can only be achieved with untruncated versions of these techniques, while decoupling of the strongest correlations can be approximately obtained with appropriate truncations. However, unlike other many-body methods, the most unique aspect of the CC similarity transformation is that because of its non-unitarity, the resulting Hamiltonian will not be Hermitian. This decoupling and non-Hermiticity can be seen in Fig. 3.3, which shows the effect of the CC similarity transformation on the Hamiltonian for a pairing case with $N = 6$ and $A = 4$. The effective Hamiltonian \bar{H} shown in Fig. 3.3 can be explicitly built, and it happens to be

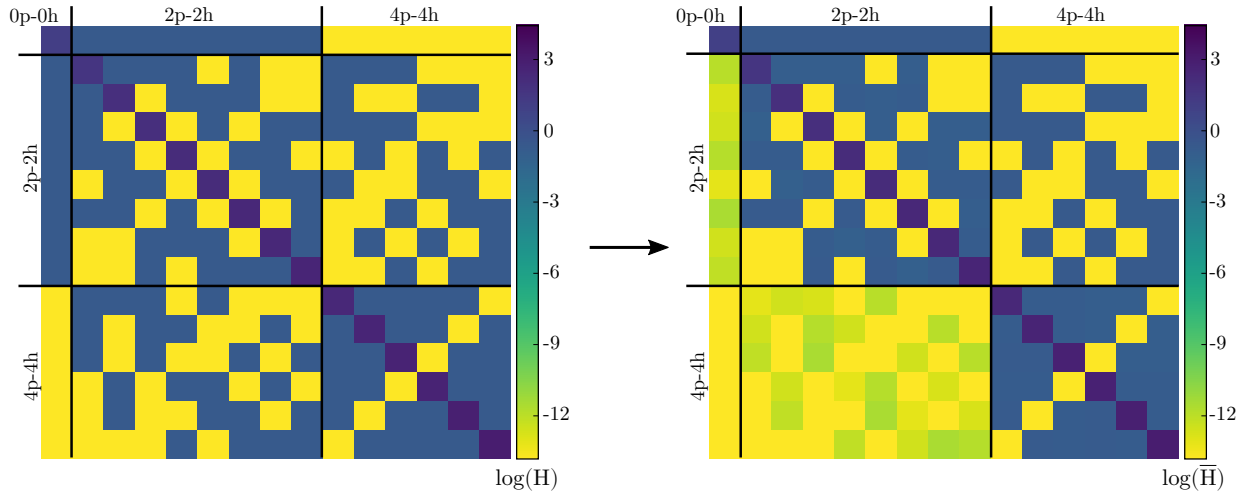


Figure 3.3: Visualization of the CCD similarity transformation on the pairing Hamiltonian for four particles and six shells. This shows the main function of CCD, which is to decouple $2p-2h$ excitations from the ground state, shown by the suppression of matrix elements on the first column. In the pairing model, this also has the effect of decoupling $2p-2h$ excitations from $4p-4h$ excitations. Also, the non-unitary nature of the transformation is obvious given the asymmetry of the resulting Hamiltonian.

beneficial to do so as part of most CC calculations, both for solving the CC equations and for use in post-CC methods. This topic is discussed in detail in the next section.

3.4 Solving the Coupled Cluster Equations

As described above, the coupled cluster equations are solved by first initializing all of the cluster amplitudes, then updating them by computing various sums over particle and hole combinations, $\text{CC}(\hat{T})$. This updating procedure is performed over multiple iterations until the amplitudes stay unchanged within a certain tolerance.

$$\begin{aligned} \text{Initialize :} \quad & \hat{T}^{(0)} = \hat{T}_{\text{init}} \\ \text{Iterate :} \quad & \hat{T}^{(n+1)} \leftarrow \text{CC}(\hat{T}^{(n)}) \end{aligned} \tag{3.24}$$

Generally, the convergence of this algorithm depends on the relative magnitudes between the inter-particle force and the single-particle energy spacing. For a relatively small Fermi gap between the closed shell of occupied states and the unoccupied particle states, the energy denominators will approach zero and cause a divergent or chaotic solution [108]. Physically, this situation occurs when a system exhibits strong many-particle clustering, which is difficult to capture with only the single and double excitations of CCSD. A simple way to avoid this ill-defined behavior is to scale the energy denominators for early iterations or to employ linear mixing to dampen the solution.

$$\hat{T}^{(n+1)} \leftarrow \alpha \text{CC}(\hat{T}^{(n)}) + (1 - \alpha) \hat{T}^{(n)} \tag{3.25}$$

If a solution to a highly-collective system does not diverge, it typically converges very slowly. To improve the convergence rate, techniques already utilized for the Hartree-Fock iterations can also be employed here, such as DIIS [91, 90] or Broyden's method [21]. The additional computational complexity for the CC iterations is simply a multiplicative factor equal to the

number of iterations performed. Typical calculations in this work with DIIS acceleration are converged within ~ 30 iterations. Therefore, any significant improvements to the CC algorithm will involve the expensive sums embedded within the function $\text{CC}(\hat{T}^{(n)})$.

3.4.1 Symmetry Channels

For the coupled cluster equations, as well as many other many-body methods, the first way to simplify the various sums is to exploit any symmetries of the underlying Hamiltonian of a particular problem. These symmetries manifest as conserved quantities, and because of the underlying nature of the cluster operators, see Section 3.2, these must conserve these quantum numbers as well. For example, the pairing Hamiltonian of Section 3.3 has a symmetry that conserves both the total spin projection and the number of pairs. The Coulomb Hamiltonian of Section 3.5, which has translational symmetry, conserves the linear momentum of any state. Finally, the spherical symmetry of the nuclear Hamiltonian ensures that angular momentum and parity are conserved. To utilize these symmetries, any sums that contain many-body states with different conserved quantum numbers can be ignored. For efficiency, these symmetry groups can be pre-sorted into *channels*, $\Sigma_{\vec{\xi}}$, where $\vec{\xi}$ represents the relevant quantum numbers of a certain channel.

For CCSD calculations, useful types of channels include the direct two-body channels, $\Sigma_{\vec{\xi}_1}$ —which categorizes the vector sum of two single-particle-state quantum numbers—and the cross two-body channels, $\Sigma_{\vec{\xi}_2}$ —which categorizes the vector difference of two single-particle-state quantum numbers or, equivalently, the vector sum of a the quantum numbers of a

single-particle state and a time-reversed single-particle state.

$$\vec{\xi}_{pq} = \vec{\xi}_p + \vec{\xi}_q \longrightarrow |pq\rangle \in \Sigma_{\vec{\xi}_1 = \vec{\xi}_{pq}} \quad (3.26)$$

$$\vec{\xi}_{p\bar{q}} = \vec{\xi}_p - \vec{\xi}_q = \vec{\xi}_p + \vec{\xi}_{\bar{q}} \longrightarrow |p\bar{q}\rangle \in \Sigma_{\vec{\xi}_2 = \vec{\xi}_{p\bar{q}}} \quad (3.27)$$

Also useful is the one-body channels, $\Sigma_{\vec{\xi}_3}$, which categorizes both single-particle states by their conserved quantum numbers. These one-body channels can also characterize a special type of three-body state: the vector difference between the quantum numbers of a direct two-body state and a single-particle state or, equivalently, the vector sum of the quantum numbers of a two-body direct state and a time-reversed single-particle state.

$$\vec{\xi}_p \longrightarrow |p\rangle \in \Sigma_{\vec{\xi}_3 = \vec{\xi}_p} \quad (3.28)$$

$$\vec{\xi}_{pq\bar{r}} = \vec{\xi}_p + \vec{\xi}_q - \vec{\xi}_r = \vec{\xi}_p + \vec{\xi}_q + \vec{\xi}_{\bar{r}} \longrightarrow |pq\bar{r}\rangle \in \Sigma_{\vec{\xi}_3 = \vec{\xi}_{pq\bar{r}}} \quad (3.29)$$

Using these channel structures, the interaction matrix elements and cluster amplitudes can be built in different ways. The full applicability of these structures are shown in detail in the appendix ??, but a few examples using sums in the CCD equations (3.3) are shown here.

$$\begin{aligned} \frac{1}{2} \sum_{cd} V_{cd}^{ab} t_{ij}^{cd} &= \frac{1}{2} \sum_{|cd\rangle} V_{cd}^{ab} t_{ij}^{cd} \text{ for } |cd\rangle \in \Sigma_{\vec{\xi}_{ab}} = \Sigma_{\vec{\xi}_{ij}} \\ \sum_{kc} V_{ic}^{kb} t_{kj}^{ac} &= \sum_{|k\bar{c}\rangle} V_{i\bar{b}}^{k\bar{c}} t_{k\bar{c}}^{a\bar{j}} \text{ for } |k\bar{c}\rangle \in \Sigma_{\vec{\xi}_{i\bar{b}}} = \Sigma_{\vec{\xi}_{a\bar{j}}} \\ \frac{1}{2} \sum_{klcd} V_{cd}^{kl} t_{ij}^{db} t_{kl}^{ca} &= \frac{1}{2} \sum_{\substack{|kl\bar{c}\rangle \\ |d\rangle}} V_d^{kl\bar{c}} t_{ij\bar{b}}^d t_{kl\bar{c}}^a \text{ for } |kl\bar{c}\rangle, |d\rangle \in \Sigma_{\vec{\xi}_{ij\bar{b}}} = \Sigma_{\vec{\xi}_a} \end{aligned} \quad (3.30)$$

3.4.2 Matrix Structures and Intermediates

Symmetry channels not only provide an organized structure for the interaction matrix elements and cluster amplitudes, and remove any terms that violate the underlying symmetry of a problem, but they also naturally provide an efficient way of performing sums using matrix-matrix multiplications. For example, the sums in Eq. (3.4.1) can be reformulated as matrix-matrix multiplications by structuring the channel-separated interaction matrix elements and cluster amplitudes into individual matrices. These operations can be performed very quickly using highly optimized linear algebra algorithms like those found in BLAS (Basic Linear Algebra Subprograms) [2]. The matrices can be reordered so that the summed indices correspond to the internal columns and rows of those matrices.

$$\begin{aligned}
\frac{1}{2} \sum_{cd} V_{cd}^{ab} t_{ij}^{cd} &= \frac{1}{2} \mathbf{V}_{cd}^{ab} \cdot \mathbf{t}_{ij}^{cd} \quad \text{for } |ab\rangle, |ij\rangle, |cd\rangle \in \Sigma_{\vec{\xi}_1} \\
\sum_{kc} V_{ic}^{kb} t_{kj}^{ac} &= \mathbf{t}_{k\bar{c}}^{a\bar{j}} \cdot \mathbf{V}_{i\bar{b}}^{k\bar{c}} \quad \text{for } |a\bar{j}\rangle, |i\bar{b}\rangle, |k\bar{c}\rangle \in \Sigma_{\vec{\xi}_2} \\
\frac{1}{2} \sum_{klcd} V_{cd}^{kl} t_{ij}^{db} t_{kl}^{ca} &= \frac{1}{2} \mathbf{t}_{kl\bar{c}}^a \cdot \mathbf{V}_d^{kl\bar{c}} \cdot \mathbf{t}_{ij\bar{b}}^d \quad \text{for } |a\rangle, |ij\bar{b}\rangle, |kl\bar{c}\rangle, |d\rangle \in \Sigma_{\vec{\xi}_3}
\end{aligned} \tag{3.31}$$

These sums correspond to different components of the updated cluster amplitudes according to Eq. (3.24). So the different channel structures of the matrix-matrix multiplications in Eq. (3.4.2) correspond to different amplitude structures according to the sum's external indices.

$$\begin{aligned}
\mathbf{t}_{ij}^{ab} &\leftarrow \frac{1}{2} \mathbf{V}_{cd}^{ab} \cdot \mathbf{t}_{ij}^{cd} \quad \text{for } |ab\rangle, |ij\rangle, |cd\rangle \in \Sigma_{\vec{\xi}_1} \\
\mathbf{t}_{i\bar{b}}^{a\bar{j}} &\leftarrow \mathbf{t}_{k\bar{c}}^{a\bar{j}} \cdot \mathbf{V}_{i\bar{b}}^{k\bar{c}} \quad \text{for } |a\bar{j}\rangle, |i\bar{b}\rangle, |k\bar{c}\rangle \in \Sigma_{\vec{\xi}_2} \\
\mathbf{t}_{ij\bar{b}}^a &\leftarrow \frac{1}{2} \mathbf{t}_{kl\bar{c}}^a \cdot \mathbf{V}_d^{kl\bar{c}} \cdot \mathbf{t}_{ij\bar{b}}^d \quad \text{for } |a\rangle, |ij\bar{b}\rangle, |kl\bar{c}\rangle, |d\rangle \in \Sigma_{\vec{\xi}_3}
\end{aligned} \tag{3.32}$$

The last summation in the matrix-matrix form of Eqs. (3.4.2) and (3.4.2) involves two multiplications, which suggests the need for an *intermediate* matrix to hold the result of the first operation. This is the last main ingredient to an efficient CC algorithm. To see the benefit of intermediate structures, it's helpful to examine an expensive sum from the CCD equations. For typical calculations, particle states outnumber hole states by an order of magnitude, $n_p \sim 10n_h$, which means that one of the most expensive sums is,

$$\frac{1}{4} \sum_{klcd} V_{cd}^{kl} t_{kl}^{ab} t_{ij}^{cd}. \quad (3.33)$$

Because this term must be computed for each t_{ij}^{ab} , its computational cost naively scales as $\mathcal{O}(N_h^4 N_p^4)$. However, using the matrix form of this sum and an intermediate matrix,

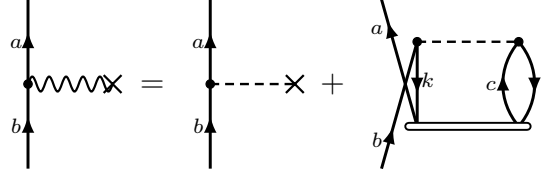
$$\frac{1}{4} \sum_{klcd} V_{cd}^{kl} t_{kl}^{ab} t_{ij}^{cd} = \frac{1}{4} \mathbf{t}_{kl}^{ab} \cdot \left(\mathbf{V}_{cd}^{kl} \cdot \mathbf{t}_{ij}^{cd} \right) = \frac{1}{4} \mathbf{t}_{kl}^{ab} \cdot \mathbf{X}_{ij}^{kl} \rightarrow \mathbf{t}_{ij}^{ab}. \quad (3.34)$$

this term is now computed as the combination of two sums, each scaling as $\mathcal{O}(N_h^4 N_p^2)$. These intermediates can also be used as a way to combine similar sums. For example, the last step of Eq. 3.34 has a very similar structure to the first sum in Eq. 3.3. Therefore, the two sums can be written with a common intermediate as,

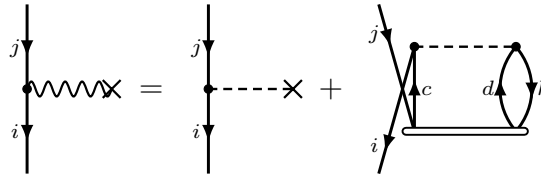
$$\begin{aligned} \frac{1}{2} \sum_{kl} V_{ij}^{kl} t_{kl}^{ab} + \frac{1}{4} \sum_{klcd} V_{cd}^{kl} t_{kl}^{ab} t_{ij}^{cd} &= \frac{1}{2} \mathbf{t}_{kl}^{ab} \cdot \left[\mathbf{V}_{ij}^{kl} + \frac{1}{2} \mathbf{V}_{cd}^{kl} \cdot \mathbf{t}_{ij}^{cd} \right] = \frac{1}{4} \mathbf{t}_{kl}^{ab} \cdot \mathbf{X}_{ij}^{kl} \rightarrow \mathbf{t}_{ij}^{ab}, \\ \text{where, } \mathbf{X}_{ij}^{kl} &= \mathbf{V}_{ij}^{kl} + \frac{1}{2} \mathbf{V}_{cd}^{kl} \cdot \mathbf{t}_{ij}^{cd} \end{aligned} \quad (3.35)$$

It just so happens that this form of the intermediate X_{ij}^{kl} is equivalent to the $hhhh$ component of the CCD similarity transformed Hamiltonian, \bar{H} . Constructing other intermediates in this way gives similar results, so it's a natural extension to actually construct

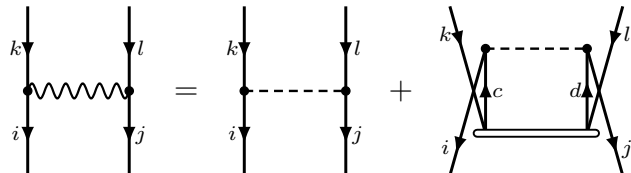
the effective Hamiltonian at each iteration for the express purpose of using it as different intermediate components for the CC equations. This has the added benefit of having already computed the effective Hamiltonian for post-CC methods. The different components of the CCD effective Hamiltonian, $\bar{H}_{\text{CCD}} = \left(\hat{H} e^{\hat{T}2} \right)_c$, are



$$X_b^a = f_b^a - \frac{1}{2} \sum_{klc} V_{bc}^{kl} t_{kl}^{ac} \quad (3.36)$$



$$X_j^i = f_j^i + \frac{1}{2} \sum_{kcd} V_{cd}^{ik} t_{jk}^{cd} \quad (3.37)$$



$$X_{kl}^{ij} = V_{kl}^{ij} + \frac{1}{2} \sum_{cd} V_{cd}^{ij} t_{kl}^{cd} \quad (3.38)$$

$$X_{jb}^{ia} = V_{jb}^{ia} - \frac{1}{2} \sum_{kc} V_{cb}^{ik} t_{jk}^{ca} \quad (3.39)$$

Using these terms, the CCSD equations can be written in pseudo-linear form. These also explicitly show the decoupling of the effective Hamiltonian with $1p$ - $1h$ and $2p$ - $2h$ excitations,

$$X_{ij}^{ab} = 0 = V_{ij}^{ab} + \hat{P}(ab) \sum_c X_c^a t_{ij}^{cb} - \hat{P}(ij) \sum_k X_i^k t_{kj}^{ab} + \frac{1}{2} \sum_{cd} X_{cd}^{ab} t_{ij}^{cd} + \frac{1}{2} \sum_{kl} X_{ij}^{kl} t_{kl}^{ab} - \hat{P}(ab|ij) \sum_{kc} X_{ic}^{kb} t_{kj}^{ac} \quad (3.40)$$

The components and intermediates of the CCSD effective Hamiltonian are much more complicated and are shown with their corresponding sums in the appendix ??.

3.5 Example: Homogeneous Electron Gas

Another relatively simple calculation using the CCD approximation is the homogeneous electron gas. This example aims to calculate the ground state energy of a three-dimensional gas of electrons subject to Coulomb repulsion. This is an approximate model of the valence

electrons in a metal, subject to a uniform background of positive charge from the nuclei and core electrons [48]. As will be explained below, this calculation employs pure-momentum eigenstates such that $1p$ - $1h$ excitations from the reference state are forbidden by momentum conservation. This means that the problem reduces to the doubles approximation. To obtain realistic results, a sufficiently-sized basis with a sufficient number of electrons must be used. Therefore, the improvements discussed in Section 3.4 are necessary to keep the computation time managable as the system size increases.

With a uniform background potential, the electron gas can be constructed using eigenfunctions of the kinetic energy operator, $^{(1)}\hat{H} = \hat{T} = \frac{-\hbar^2}{2m}\nabla^2$. In an infinite volume, however, there are an unlistable number of plane wave modes which satisfy this condition due to the continuous nature of the linear momentum eigenstates. Therefore, the single-particle orbits will be constructed in a finite box of volume Ω and length L , and then the limit $L \rightarrow \infty$ can be taken after various expectation values have been computed.

$$\begin{aligned}\frac{-\hbar^2}{2m}\nabla^2\phi_{\mathbf{k}\sigma}(\mathbf{r}) &= \epsilon_{\mathbf{k}}\phi_{\mathbf{k}\sigma}(\mathbf{r}) \\ \phi_{\mathbf{k}\sigma}(\mathbf{r}) &= \frac{1}{\sqrt{\Omega}}\exp(i\mathbf{k}\mathbf{r})\xi_{\sigma}\end{aligned}\tag{3.41}$$

where m is the electron mass, \mathbf{k} is the wave number, and ξ_{σ} is the spin function for either spin up or down electrons

$$\xi_{\sigma=+1/2} = \begin{pmatrix} 1 \\ 0 \end{pmatrix} \quad \xi_{\sigma=-1/2} = \begin{pmatrix} 0 \\ 1 \end{pmatrix}.\tag{3.42}$$

Assuming the single-particle orbits follow periodic boundary conditions within the con-

taining box ($\phi(\mathbf{r}_i) = \phi(\mathbf{r}_i + L)$ for $i = x, y, z$) the wave numbers are quantized,

$$k_i = \frac{2\pi n_i}{L} \quad i = x, y, z \quad n_i = 0, \pm 1, \pm 2, \dots \quad (3.43)$$

A state can therefore be characterized by the quantum numbers n_x , n_y , and n_z as well as the spin quantum number σ . The energy of such a state, independent of the spin, can be written as

$$\epsilon_{n_x, n_y, n_z} = \frac{\hbar^2}{2m} (k_x^2 + k_y^2 + k_z^2) = \frac{\hbar^2}{2m} \left(\frac{2\pi}{L} \right)^2 (n_x^2 + n_y^2 + n_z^2). \quad (3.44)$$

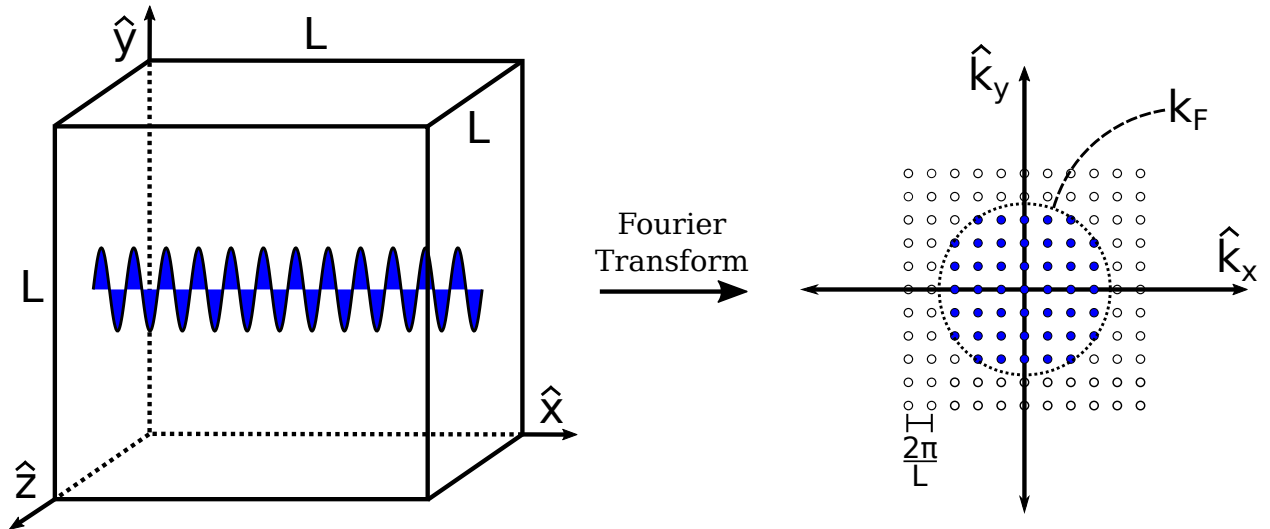


Figure 3.4: Visualization of the Fourier transform of a finite box. This transformation characterizes the construction of the single-particle basis for infinite matter, mapping plane waves in coordinate space onto finitely-spaced points in momentum space.

Now that the single-particle orbits are established, a particular basis consisting of these orbits can be chosen such that all states are included up to a closed shell. This basis is then filled with electrons until a closed Fermi level is obtained. Additionally, only the unpolarized case, in which all orbitals are occupied with one spin-up and one spin-down electron, will be

considered here. For this spherical-type level structure, the number of electrons required for closed shells increases quickly. For example, the first six shells contain 2, 14, 38, 54, 66 and 114 states, respectively.

A finite number of electrons A in a finite box of volume Ω naturally leads to the characterization of an infinite system by its number density $\rho = A/\Omega$. The average inter-electron distance, or *Wigner-Seitz radius*, is defined as

$$\frac{4}{3}\pi r_s^3 = \frac{1}{\rho}, \quad r_s = \left(\frac{3}{4\pi\rho} \right)^{1/3}. \quad (3.45)$$

In practice, these calculations are defined by the total number of shells included in the basis, the number of electrons, and the Wigner-Seitz radius, usually given in units of the Bohr radius, $r_b = \frac{\hbar}{mc\alpha}$, where c is the speed of light and α is the fine-structure constant.

The last ingredient to this many-body calculation is the interaction between the electrons, the well-known Coulomb force. Using atomic units, where the elementary charge $e = 1$ and the Coulomb constant $\frac{1}{4\pi\epsilon_0} = 1$, this potential is simply

$$V(\mathbf{r}_1, \mathbf{r}_2) = \frac{1}{|\mathbf{r}_1 - \mathbf{r}_2|}. \quad (3.46)$$

As mentioned in chapter 2, this potential can be utilized in second-quantization by computing antisymmetrized integrals over the basis states. In this case, the integrals have the form,

$${}^{(2)}H_{rs}^{pq} \equiv \int d\mathbf{r}_1 d\mathbf{r}_2 \phi_{\mathbf{k}_p\sigma_p}^*(\mathbf{r}_1) \phi_{\mathbf{k}_q\sigma_q}^*(\mathbf{r}_2) \frac{1}{|\mathbf{r}_1 - \mathbf{r}_2|} [\phi_{\mathbf{k}_r\sigma_r}(\mathbf{r}_1) \phi_{\mathbf{k}_s\sigma_s}(\mathbf{r}_2) - \phi_{\mathbf{k}_s\sigma_s}(\mathbf{r}_1) \phi_{\mathbf{k}_r\sigma_r}(\mathbf{r}_2)]. \quad (3.47)$$

The symmetries of the Coulomb potential guarantee that the total linear momentum and

total spin projection are conserved such that,

$$\mathbf{k}_p + \mathbf{k}_q = \mathbf{k}_r + \mathbf{k}_s \quad \text{and} \quad \sigma_p + \sigma_q = \sigma_r + \sigma_s. \quad (3.48)$$

The integral is relatively simple given the form of the basis functions. The result is given in terms of the momentum transfer, $\mathbf{q}_1 = \mathbf{k}_p - \mathbf{k}_r$ and $\mathbf{q}_2 = \mathbf{k}_p - \mathbf{k}_s$,

$${}^{(2)}H_{rs}^{pq} = \frac{4\pi\hbar c\alpha}{\Omega} \left[\frac{\delta_{\sigma_p\sigma_r}\delta_{\sigma_q\sigma_s}}{|\mathbf{q}_1|^2} - \frac{\delta_{\sigma_p\sigma_s}\delta_{\sigma_q\sigma_r}}{|\mathbf{q}_2|^2} \right] \quad (3.49)$$

The last preparation step before performing the coupled cluster algorithm is the Hartree-Fock transformation. As with the pairing model, the single-particle orbitals are already eigenfunctions of the Fock operator, and thus the transformation consists simply of redefining the single-particle energies while the two-body interaction is left unchanged.

$$\begin{aligned} \varepsilon_p &= \epsilon_{\mathbf{k}_p} + \sum_i {}^{(2)}H_{pi}^{pi} \\ V_{rs}^{pq} &= {}^{(2)}H_{rs}^{pq} \end{aligned} \quad (3.50)$$

As mentioned above, in the plane-wave basis, any single excitation from the reference state vanishes automatically due to momentum conservation, $t_i^a = 0$. Therefore, it's necessary to include only double excitations (before adding triples, etc.). Using the pseudo-linear form of the CCD equations (??) and an effective Hamiltonian that excludes single excitations in Eqns. (3.36)-(??). The total energy per electron can now be calculated and plotted as a function of the Wigner-Seitz radius. In the limit $N, L \rightarrow \infty$, the plot in Fig. 3.5 represents the equation-of-state for a 3D electron gas at absolute zero. This curve can reveal many thermodynamic properties of the electron gas including the saturation density and satura-

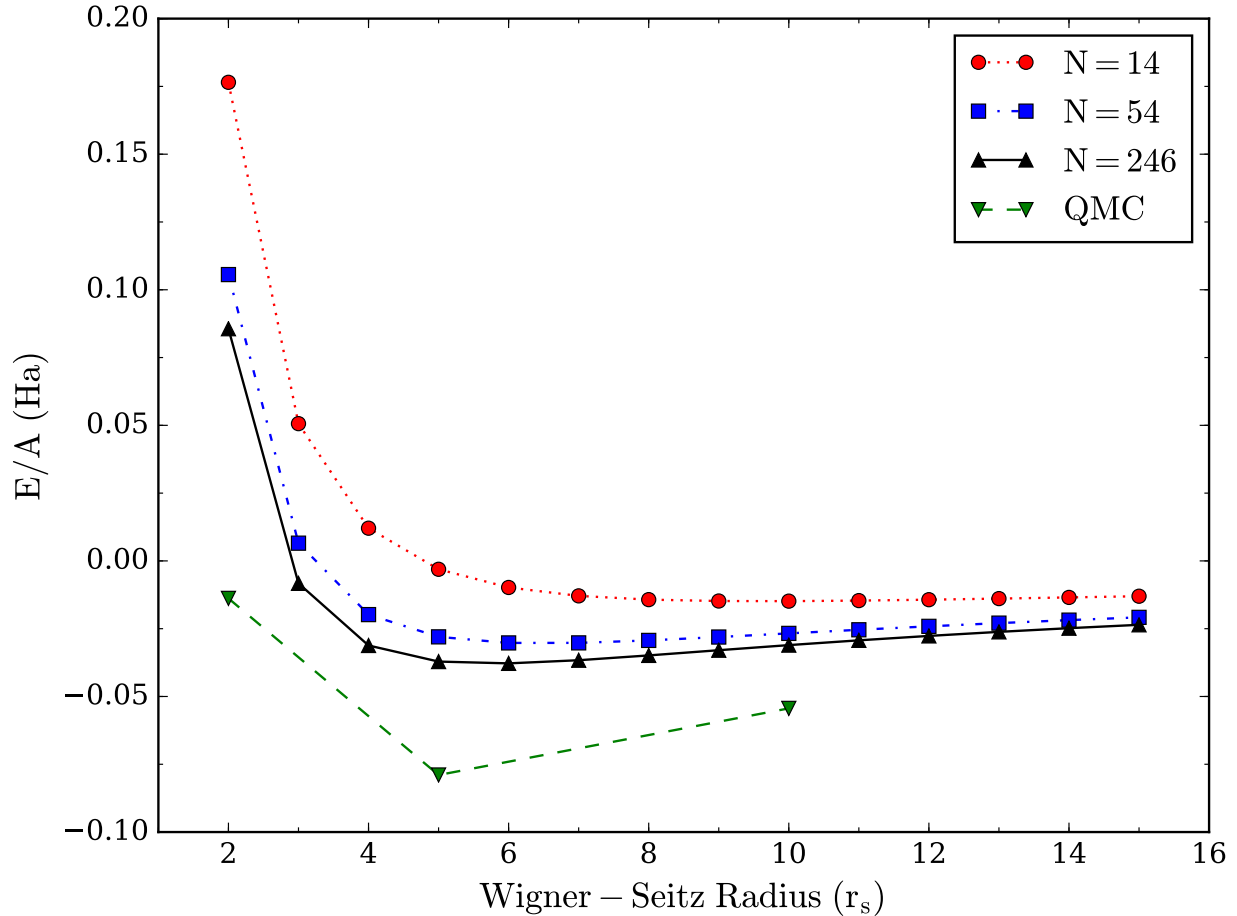


Figure 3.5: CCD energy per electron in Hartrees for the 3D homogeneous electron gas as function of the Wigner-Seitz radius in units of Bohr radii. The calculation used periodic boundary conditions and a basis with 25 shells, resulting in a total of 1238 single-particle states. Also plotted are the variational quantum Monte Carlo (QMC) results from [75].

tion energy, which occur at the lowest point on the curve. The CCD results are compared with the quasi-exact results from variational quantum Monte Carlo calculations from [75]. The discrepancies between the saturation energies from the two methods can be partially attributed to an insufficient basis size. However, even an appropriate extrapolation to an infinite basis won't be able to recover all of the required correlations, which suggests that CCSDT might be necessary. Regardless of the value to the saturation energy, these CCD results do qualitatively reproduce the saturation radius at $r_s \approx 5.0$.

3.6 Coupled Cluster for Finite Nuclei

The main purpose of this work is to calculate properties of atomic nuclei with coupled cluster theory. From a many-body perspective, the main process is computing the converged cluster amplitudes and thus the important correlations of the system. These amplitudes comprise the CC similarity transformation, which is versatile for constructing any effective operator, such as the Hamiltonian, that can act on the correlated system. Therefore, the first step in calculating beta-decay properties of nuclei is solving for the ground-state wave function of specific closed-shell nuclei.

3.6.1 Harmonic Oscillator Basis

Calculations of finite nuclei follow the basic structure of the algorithms used for the pairing model and the homogeneous electron gas, but they also differ in some significant ways. Like the other examples, the first step is to construct a proper single-particle basis and reference state. Because the nuclear Hamiltonian conserves angular momentum and parity, it's useful to construct orbits that are eigenfunctions of these operators. For a system with no external potential, like the electron gas, this suggests a basis made of plane waves. However, plane waves do not represent the bound states of a nucleus very well. This property can be satisfied by introducing a fictitious external potential that mimics the mean field from the collection of nucleons. Some phenomenological potentials, like the Woods-Saxon potential, properly consider the resonance and continuum states of realistic nuclei in addition to the bound states. Many-body techniques discussed in this work have been applied to model spaces that include all three types of single-particle states [78, 50] with some success. However, for the many-body states considered in this work, it's sufficient to consider only bound single-particle states. Therefore, the nuclear basis will be constructed from the isotropic harmonic

oscillator,

$$V(r) = \frac{1}{2}m\omega^2 r^2. \quad (3.51)$$

An eigenstate of the harmonic oscillator potential is defined by its principal quantum number n and its orbital angular momentum quantum number l , which is denoted by the letters s, p, d, f... for the values $l = 0, 1, 2, 3...$ respectively. Because of spin-orbit terms in the nuclear Hamiltonian, the orbital angular momentum is coupled to a particle spin to a total angular momentum of $j = |\mathbf{l} + \mathbf{s}|$, which results in a degeneracy of $2j + 1$ for each orbit. This basis does not provide any simplification to eliminate single excitations, so CCSD will be used for all the following calculations. A schematic version of this single-particle basis is shown in Fig. 3.6. The shell structure of this basis is characterized by the energy quantum numbers, $e = 2n + l$, of the HO single-particle spectrum. This can be used to define the maximum-energy shell and the size of a HO basis with the number e_{\max} .

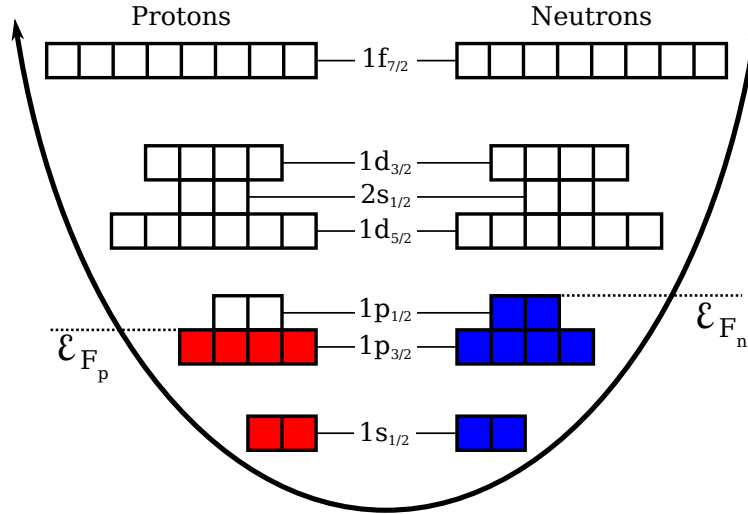


Figure 3.6: A schematic illustration of the harmonic oscillator basis used for calculations of nuclei. Shown is an example of a initial reference state for carbon-14, with 6 protons filled to the $p_{3/2}$ -subshell closure and 8 neutrons filled to the $p1$ -shell closure. See text for details on the single-particle states.

One issue with this construction, is that while the single-particle orbits are eigenstates of

the angular momentum operator and localized to the external potential, they are not translationally invariant, which is required by the nuclear Hamiltonian. This means that there is a fictitious center-of-mass kinetic energy which must be removed from the Hamiltonian. The COM kinetic energy can be written as the sum of one- and two-body pieces,

$$\hat{T}_{\text{cm}} = \frac{\mathbf{P}_{\text{cm}}^2}{2mA} = \sum_{pq} \frac{\mathbf{p}_p \cdot \mathbf{p}_q}{2mA} = \sum_p \frac{\mathbf{p}_p^2}{2mA} + \sum_{p < q} \frac{\mathbf{p}_p \cdot \mathbf{p}_q}{mA}. \quad (3.52)$$

The one-body piece is just a scaled form of the original kinetic energy operator, and the two-body piece is given in a similar form to the original two-body Hamiltonian. Both can be integrated into matrix elements like Eq. (2.2),

$$\begin{aligned} {}^{(1)}T_q^p &\equiv \int d\mathbf{r}_1 \phi_p^*(\mathbf{r}_1) \frac{\mathbf{p}_1^2}{2mA} \phi_q(\mathbf{r}_1) \\ {}^{(2)}T_{rs}^{pq} &\equiv \int d\mathbf{r}_1 d\mathbf{r}_2 \phi_p^*(\mathbf{r}_1) \phi_q^*(\mathbf{r}_2) \frac{\mathbf{p}_1 \cdot \mathbf{p}_2}{mA} [\phi_r(\mathbf{r}_1) \phi_s(\mathbf{r}_2) - \phi_s(\mathbf{r}_1) \phi_r(\mathbf{r}_2)] \end{aligned} \quad (3.53)$$

Subtracting the COM kinetic energy results in the *intrinsic* Hamiltonian for finite nuclear systems,

$$\begin{aligned} \hat{H}_{\text{in}} = & \left(1 - \frac{1}{A}\right) \sum_{pq} {}^{(1)}T_q^p \hat{a}_p^\dagger \hat{a}_q + \frac{1}{4} \sum_{pqrs} \left({}^{(2)}H_{rs}^{pq} - {}^{(2)}T_{rs}^{pq} \right) \hat{a}_p^\dagger \hat{a}_q^\dagger \hat{a}_s \hat{a}_r \\ & + \frac{1}{36} \sum_{pqrstu} {}^{(3)}H_{stu}^{pqr} \hat{a}_p^\dagger \hat{a}_q^\dagger \hat{a}_r^\dagger \hat{a}_u \hat{a}_t \hat{a}_s + \dots, \end{aligned} \quad (3.54)$$

This form of the bare Hamiltonian (up to the three-body force) is used in the Hartree-Fock transformation. Then, after normal-ordering, the three-body piece is discarded, which is referred to as a NN+3N-induced interaction. The use of a localized external potential has further complications involving the COM wave function that are discussed in section 3.7.

A special property of this single-particle basis that can be exploited to reduce the computational complexity of the problem is the degeneracy of each orbital, due to the angular momentum projection of each single-particle state, $m_j = \{-j, -j+1, \dots, j-1, j\}$. According to the Wigner-Eckart theorem, the geometrical component of a wave function, dependent on its projection m_j , can be isolated as a Clebsch-Gordon coefficient. Because these coefficients have compact summation rules, any diagram and corresponding sum can be written in terms of the j -orbitals instead of the single-particle m_j states, commonly known as J -scheme and M -scheme, respectively. Calculations in J -scheme require complicated angular momentum coupling, detailed in the appendix ??, but involve roughly an order of magnitude fewer states compared with an M -scheme calculation in the same model space.

3.6.2 The Nuclear Interaction

Perhaps the most important component in nuclear structure calculations, and also perhaps the most easily overlooked component from a many-body perspective, is the nuclear Hamiltonian. Further complicated by the composite nature of protons and neutrons, bound by gluon exchange within the nucleon, the inter-nucleon interaction is a residual force of virtual pion exchanges and other, more exotic processes. Early ab initio calculations avoided this complexity by using phenomenological interactions, tuned to reproduce certain properties of a nucleus. These phenomenological forces were effectively used for calculations using shell-model CI and density-functional theory, but were restricted by the conditions of the fitted parameters.

These problems, along with the success of quantum field theories in high-energy physics, motivated the effort to describe the inter-nucleon interaction in terms of the underlying quantum chromodynamics (QCD). However, while calculations of nuclei in terms of their

constituent quarks using lattice QCD have made some progress with increases in computing power, they have been confined to few nucleon systems [8]. The problem is finding a way to express the high-energy QCD interactions as low-energy forces between nucleons. Such a problem, containing two vastly different scales, can be rewritten as an effective theory.

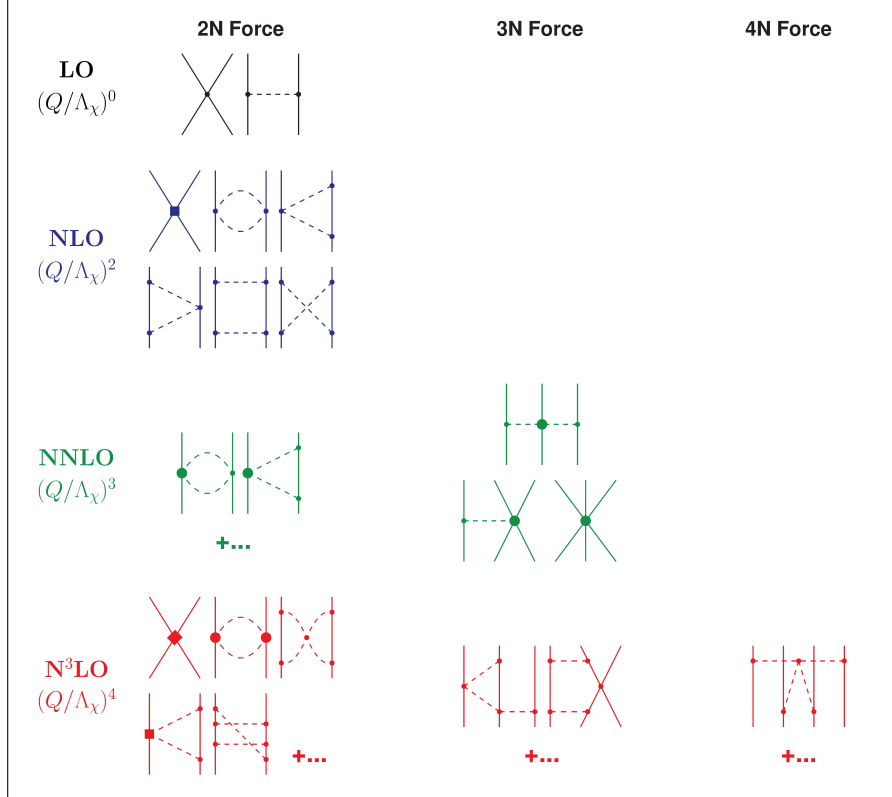


Figure 3.7: Diagrammatic form of the chiral EFT expansion up to $N^3\text{LO}$. The solid lines represent nucleons and the dashed lines represent pions. The different vertices represent higher-order interactions. Figure taken from [77].

Chiral effective field theory (EFT), which exploits the large difference in scales between the low-energy regime of nuclear physics and the high-energy regime of QCD, is built from a general Lagrangian consistent with the broken chiral symmetry of QCD [39, 77]. This broken symmetry, a consequence of non-zero quark masses, results in several hadronic structures including protons, neutrons, and mesons, the lightest of which is the pion, $m_\pi \approx 140\text{MeV}/c^2$ [10]. This can be exploited by systematically writing a Lagrangian as the sum of pion

exchanges of increasing order. Additional contact interactions, which represent exchanges of heavier mesons, are also included and must be fit to low-energy nuclear data. The hierarchy of EFT terms, which contain 3N and higher many-body forces, are ordered by power counting the expansion term (m_π/Λ) , where Λ is an energy cutoff between the low- and high-energy scales, and is shown up to N³LO in Fig. 3.7.

This work exclusively employs the NN force of the N³LO interaction from Entem and Machleidt with a cutoff of $\Lambda = 500$ MeV [38]. For most calculations, this interaction is coupled with the N³LO 3N interaction from Navrátil with a cutoff of $\Lambda = 400$ MeV [82]. This NN+3N(400) interaction is successful at reproducing low- and medium-mass nuclei, but begins to overbind beyond the *sd*-shell. As mentioned in the introduction, these bare Hamiltonians exhibit strong repulsion at short ranges among high-momentum states. Therefore to soften the interaction, the similarity renormalization group method is used to integrate high-momentum modes out of the interaction while preserving observables [17, 94].

3.6.3 Ground-State Results for Nuclei

The main object of this section is to demonstrate the validity of all the ingredients which have been discussed so far: the harmonic oscillator basis, the NN+3N(400) chiral interaction, and the *J*-scheme CCSD algorithm. To accomplish this, calculations for different nuclei will be compared to the corresponding experimental values. Additionally, results for different input parameters will be presented to verify that the observables are independent of non-physical variables. Once again, all results are computed with a HF-optimized basis, see section 2.5.

First, the ground-state energies should be independent of the SRG cutoff parameter λ_{SRG} . While the SRG evolution should preserve any observables, the renormalization process

induces 3N and higher-body forces which can be missed by truncations of the many-body method in both the cluster amplitudes and the Hamiltonian. The trade-off here is that larger cutoff parameters produce interactions that contain higher-momentum components, which reduce a system's convergence properties, but induce fewer many-body forces, so that systems can be accurately described with fewer correlations. Conversely, a smaller cutoff parameter means that solutions can be more easily converged but necessitates a many-body method that includes more correlations or higher-order forces [93]. To show this effect, the ground state for oxygen-16 is shown for different cutoff parameters and for both the NN and NN+3N-induced interactions. Accounting for both the small dependence on the SRG cutoff parameter and the minor inaccuracies from the truncations made to the cluster operator and the Hamiltonian, the rest of this work will use the NN+3N(400)-induced interaction with an SRG cutoff parameter of $\lambda_{\text{SRG}} = 2.0 \text{ fm}^{-1}$.

Next, any nuclear observables calculated with this framework should be independent of the fictitious confining potential. This can be verified by showing the ground-state energies of various nuclei as a function of the underlying harmonic oscillator energy, $\hbar\omega$. Convergence is reached by increasing the size of the model space until the resulting curve is flat. Fig. 3.9 shows the convergence for the *doubly-magic*, $N = Z$ nuclei, ^4He , ^{16}O , ^{20}Ca , and ^{56}Ni , where both protons and neutrons fill the same major shell closure. All the results converge to a variance of $< 1\%$ at $e_{\text{max}} = 12$ for intermediate values of $\hbar\omega$. While a larger model space is always desirable, this level of variance justifies the use of $e_{\text{max}} = 12$ for post-CC calculations. Additionally, these results show the limitations of the NN+3N(400) interaction, as overbinding increases with the system size, where the ground-state energies of ^{20}Ca and ^{56}Ni differ from their experimental binding energies by $\sim 8\%$ and $\sim 13\%$, respectively.

The ground-state results are also shown for singly-magic nuclei, where either the protons

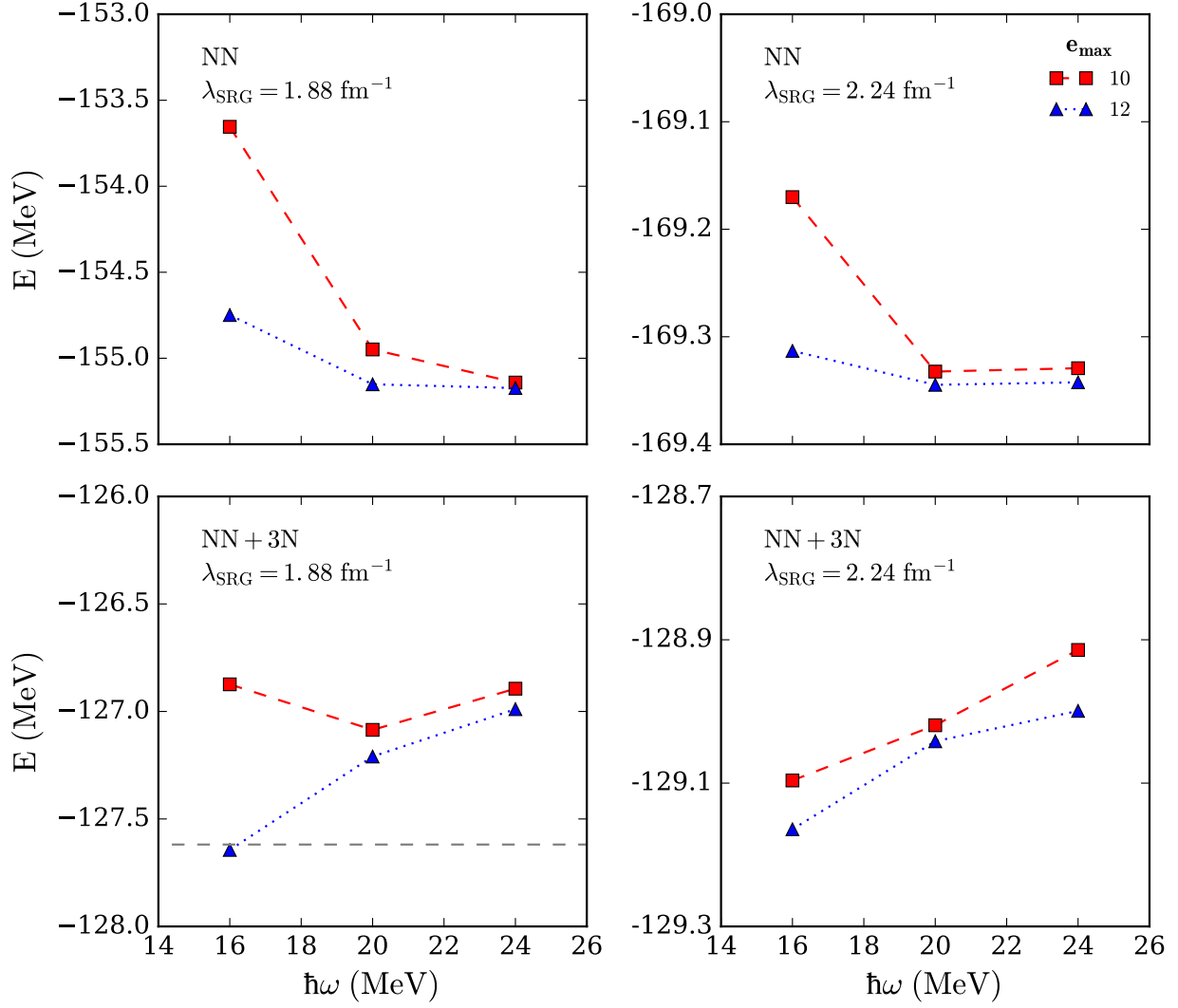


Figure 3.8: Ground-state energies for ^{16}O for the EM N^3LO NN only interaction and with the added 3N interaction from Navrátil, both SRG softened with $\lambda_{\text{SRG}} = 1.88, 2.24 \text{ fm}^{-1}$. The energies are plotted for $e_{\text{max}} = 10, 12$. The most obvious difference is between the NN and NN+3N calculations, showing the importance of including 3N forces. The differences between the cutoff parameters are resolved within $\sim 1\%$ with the inclusion of 3N forces and can be rectified further by including additional correlations or full 3N forces. The experimental binding energy is shown with the grey dashed line.

or neutrons fill a sub-shell closure. This has the potential complication of a vanishing energy gap between the hole and particle states, like the picture in Fig. ??, which causes undefined behavior in the CC algorithm (see section 3.4). However, the subshell orbitals repel each other when transformed during the Hartree-Fock algorithm, so these systems are valid in

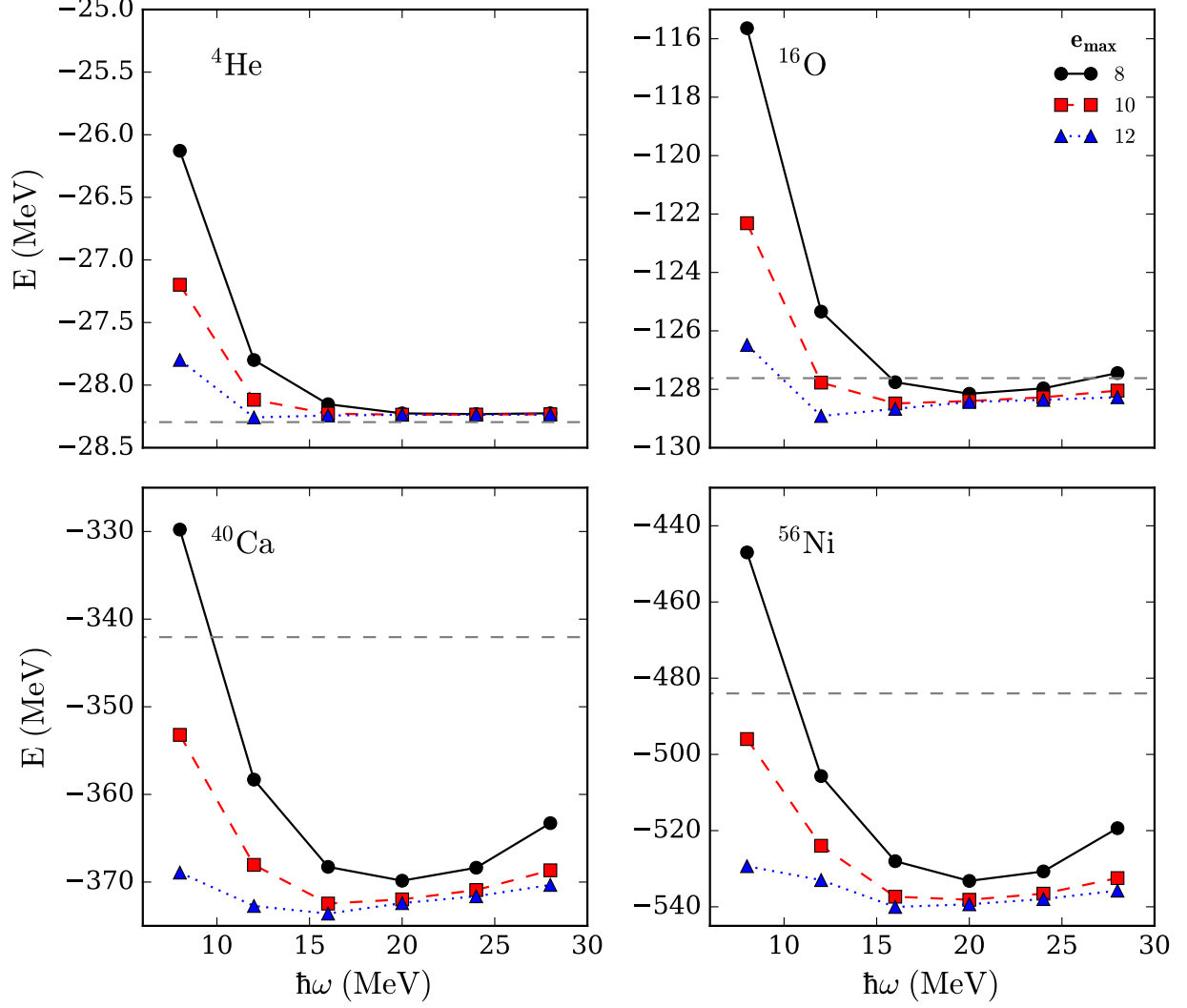


Figure 3.9: Ground-state energies for doubly magic nuclei as a function of the harmonic oscillator energy $\hbar\omega$ with the NN+3N(400) interaction, SRG softened with $\lambda_{\text{SRG}} = 2\text{fm}^{-1}$. The energies are plotted for $e_{\text{max}} = 8, 10, 12$, showing the convergence as the model space increases. The results are independent of the underlying oscillator frequency to $\sim 1\%$ for $e_{\text{max}} = 12$. The grey dashed line is the experimental binding energy. The overbinding of this interaction becomes apparent as the system size increases.

some cases. The ground-state energies for ${}^{14}\text{C}$, ${}^{22}\text{O}$, and ${}^{34}\text{Si}$ are plotted as a function of the underlying oscillator potential in Fig. 3.10. The smaller energy gap involved in these systems results in stronger excitations missed by the CCSD approximation, which cause further deviations from the experimental values.

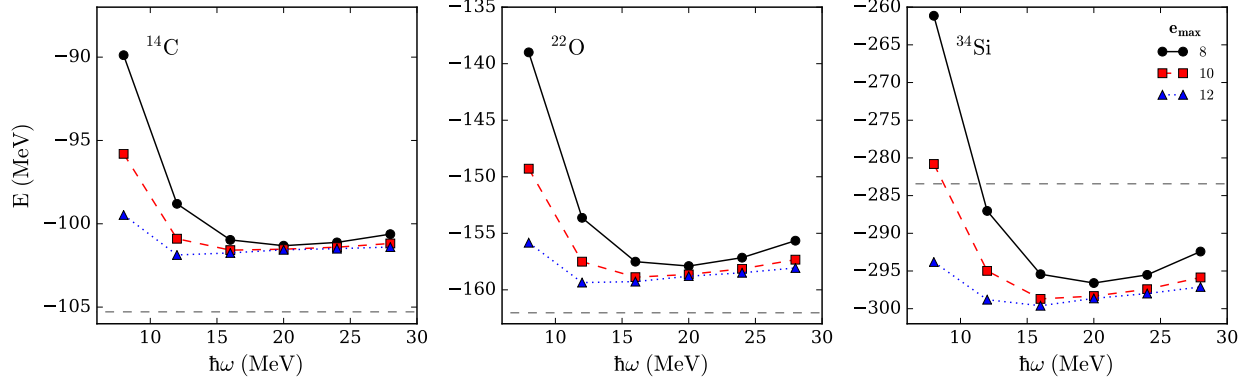


Figure 3.10: Ground-state energies for singly magic nuclei as a function of the harmonic oscillator energy $\hbar\omega$ with the NN+3N(400) interaction, SRG softened with $\lambda_{\text{SRG}} = 2\text{fm}^{-1}$. The energies are plotted for different e_{max} . The results are independent of the underlying oscillator frequency to $\sim 1\%$ for $e_{\text{max}} = 12$. The grey dashed line is the experimental binding energy. These results underbind with respect to their doubly-magic counterparts in Fig. 3.9.

3.7 Ground-State Center-of-Mass Factorization

While an intrinsic Hamiltonian can be built by removing the center-of-mass (COM) kinetic energy, Eq. (3.54), there is still an inconsistency between the translational invariance of the underlying harmonic oscillator basis and translationally-invariant nuclear many-body states [74, 46]. This inconsistency can materialize in certain calculations in the form of spurious, non-physical states.

Of course, this problem can be avoided by using more complicated basis states that obey translational invariance, such as the use of Jacobi coordinates. but such methods are limited to few-body problems [14, 85]. Another possible solution is to use the harmonic oscillator basis in an untruncated space of Slater determinants up to a certain harmonic oscillator shell. Known as the N_{max} space, this treatment can be successfully applied within no-core shell model calculations [84]. However, the factorial scaling of this method restricts its use to light nuclei. It can be shown that in the N_{max} space, the eigenstates of the intrinsic Hamiltonian are also eigenstates of the COM Hamiltonian, and any state perfectly factorizes into a COM

component and a translationally-invariant, intrinsic component,

$$|\Psi\rangle = |_{\text{in}}\rangle |_{\text{cm}}\rangle. \quad (3.55)$$

This factorization results in a compound energy spectrum, where the intrinsic component of the spectrum is degenerate for each COM excitation. Therefore, the intrinsic spectrum can be recovered by offsetting the COM Hamiltonian by the corresponding excitation energies, such that the COM energies vanish, $E_{\text{cm}} = 0$. However, with truncated methods like CCSD, this factorization is not guaranteed, and COM energies, no longer eigenenergies of the COM Hamiltonian, can take on values $E_{\text{cm}} \neq 0$. In this case, the intrinsic spectrum is contaminated with nonphysical, *spurious* states.

Because the specific form is irrelevant [118], the shifted COM Hamiltonian can be assumed to take the form of a harmonic trap with a oscillator strength of $\hbar\tilde{\omega}$, not necessarily equal to the oscillator strength of the underlying basis $\hbar\tilde{\omega}$,

$$\hat{H}_{\text{cm}}(\tilde{\omega}) = \frac{\mathbf{P}_{\text{cm}}^2}{2mA} + \frac{1}{2}mA\tilde{\omega}^2\mathbf{R}_{\text{cm}}^2 - \frac{3}{2}\hbar\tilde{\omega}, \quad (3.56)$$

offset by the ground-state energy, $\frac{3}{2}\hbar\tilde{\omega}$. In the N_{max} space, the factorization in Eq. (3.55) occurs regardless of $\hbar\tilde{\omega}$, while in truncated methods like CCSD, the COM oscillator strength is a free parameter which can be used to probe the level of COM contamination. If a frequency exists such that $E_{\text{cm}}(\tilde{\omega}) \approx 0$, then the wave function is approximately factorized, and the COM wave function is in its ground state [52, 64].

The COM energy, E_{cm} , can be calculated by using a version of the Hellmann-Feynman theorem by adding the COM Hamiltonian as a perturbation and computing the difference

quotient [34, 40],

$$E_{\text{cm}}(\tilde{\omega}) \equiv \langle |\hat{H}_{\text{cm}}| \rangle \approx \frac{1}{2\delta} \left(\langle |\hat{H} + \delta\hat{H}_{\text{cm}}(\tilde{\omega})| \rangle - \langle |\hat{H} - \delta\hat{H}_{\text{cm}}(\tilde{\omega})| \rangle \right). \quad (3.57)$$

Because the operator \mathbf{R}_{cm} depends only on the underlying single-particle basis regardless of the COM oscillator frequency, it can be rewritten in terms of \hat{H}_{cm} to find the relationship between ω and $\tilde{\omega}$,

$$\frac{1}{\tilde{\omega}^2} \left(\hat{H}_{\text{cm}}(\tilde{\omega}) - \hat{T}_{\text{cm}} + \frac{3}{2}\hbar\tilde{\omega} \right) = \frac{1}{\omega^2} \left(\hat{H}_{\text{cm}}(\omega) - \hat{T}_{\text{cm}} + \frac{3}{2}\hbar\omega \right). \quad (3.58)$$

Using the known value $\langle |\hat{T}_{\text{cm}}| \rangle = \frac{3}{4}\hbar\tilde{\omega}$ and the requirement that $E_{\text{cm}}(\tilde{\omega}) = 0$ gives the following relation that relates the COM oscillator frequency to the underlying basis frequency,

$$\hbar\tilde{\omega} = \hbar\omega + \frac{2}{3}E_{\text{cm}}(\omega) \pm \sqrt{\left(\frac{2}{3}E_{\text{cm}}(\omega)\right)^2 + \frac{4}{3}\hbar\omega E_{\text{cm}}(\omega)}. \quad (3.59)$$

The ground-state COM energies are plotted for ^{16}O and ^{40}Ca using the COM Hamiltonian with two different oscillator strengths in Fig. 3.11: that of the underlying basis, $\hbar\omega$, and one of the two solutions to Eq. (3.59), $\hbar\tilde{\omega}_{\pm}$. Of the two $\hbar\tilde{\omega}_{\pm}$, which are shown as the solutions to Eq. (3.59) in the inset, one typically results in a large COM energy while the other vanishes, which is plotted. Because the COM energies approximately vanish regardless of the underlying basis frequency, the COM wave function is in its ground state and approximately factorized from the intrinsic nuclear wave function.

Unfortunately, when intrinsic states are coupled to COM excited-states, they can contaminate the spectrum of intrinsic states coupled to the COM ground-state. These spurious states can be essentially removed from the ground-state spectrum with the Lawson-Gloeckner

method [46]. When the proper COM oscillator strength is chosen such that the COM ground-state energy vanishes, the COM Hamiltonian can be added to the intrinsic Hamiltonian at an arbitrarily large scale, β , without changing the ground-state spectrum,

$$\hat{H}_{\text{in}} \rightarrow \hat{H}_{\text{in}} + \beta \hat{H}_{\text{cm}}. \quad (3.60)$$

When β is arbitrarily large, eigenenergies of intrinsic states coupled to COM excited states will increase by the COM energy quanta, $\beta \hbar \tilde{\omega}$, such that they are removed from the range of low-lying states of interest. The method will be used to remove spurious states from the spectra of open-shell states in section ??.

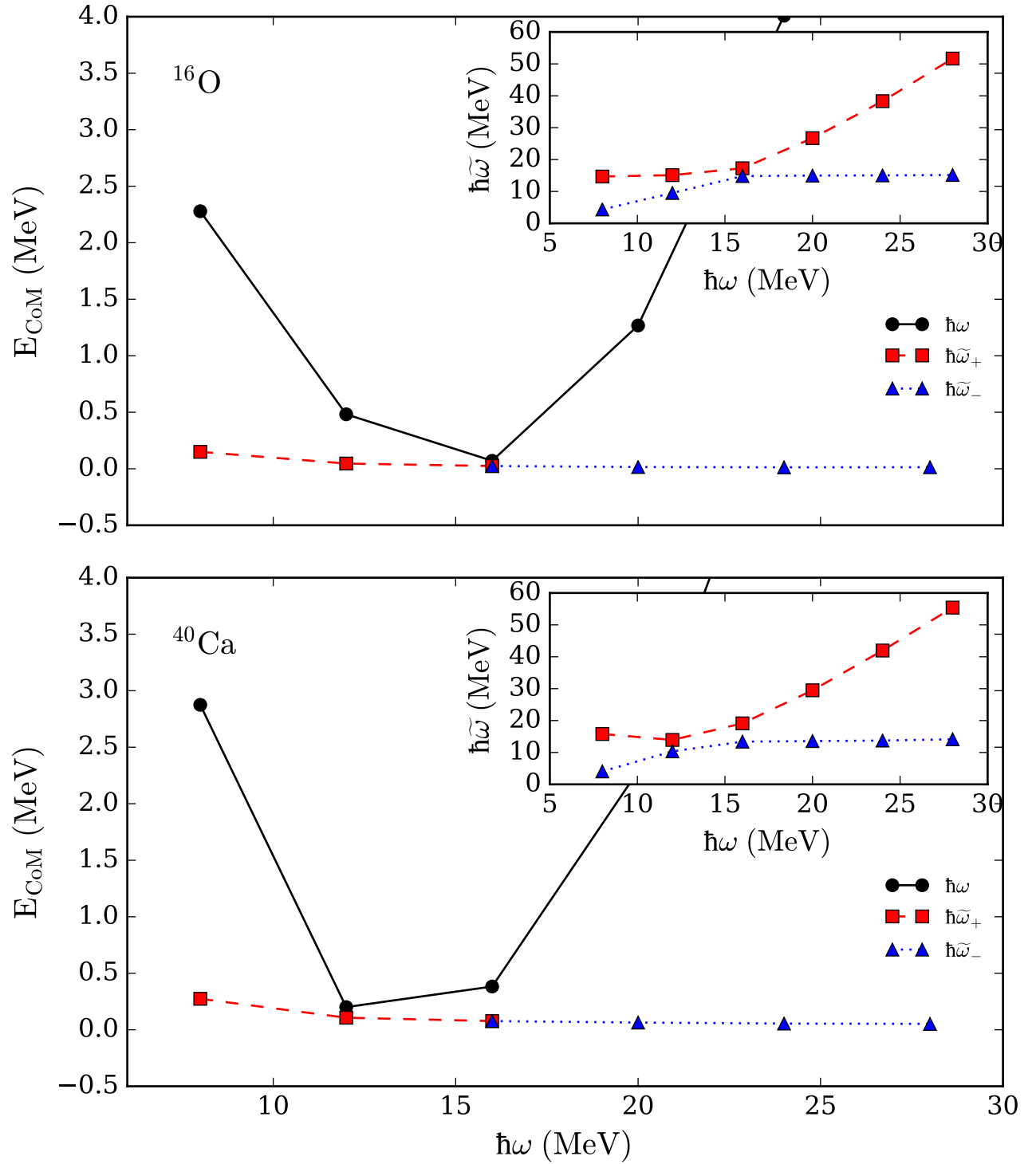


Figure 3.11: Ground-state COM energies, Eq. (3.56), for ^{16}O and ^{40}Ca at varies harmonic oscillator frequencies with the NN+3N(400)-induced with $\lambda_{\text{SRG}} = 2.0 \text{ fm}^{-1}$ at $e_{\text{max}} = 12$. Using the proper COM oscillator frequencies shows the approximate factorization of Eq. (3.55).

REFERENCES

REFERENCES

- [1] Derivation of the brueckner many-body theory. *Proceedings of the Royal Society of London A: Mathematical, Physical and Engineering Sciences*, 239(1217):267–279, 1957.
- [2] An updated set of basic linear algebra subprograms (blas). *ACM Trans. Math. Softw.*, 28:135, 2002.
- [3] Frank T. Avignone, Steven R. Elliott, and Jonathan Engel. Double beta decay, majorana neutrinos, and neutrino mass. *Rev. Mod. Phys.*, 80:481–516, Apr 2008.
- [4] R. F. Bacher. The interaction of configurations: $sd - p^2$. *Phys. Rev.*, 43:264–269, Feb 1933.
- [5] F.C. Barker, B.A. Brown, W. Jaus, and G. Rasche. Determination of $\nu\nu$ from fermi decays and the unitarity of the km-mixing matrix. *Nuclear Physics A*, 540(3):501 – 519, 1992.
- [6] Bruce R. Barrett, Petr Navrátil, and James P. Vary. Ab initio no core shell model. *Progress in Particle and Nuclear Physics*, 69(Supplement C):131 – 181, 2013.
- [7] Rodney J. Bartlett and Monika Musiał. Coupled-cluster theory in quantum chemistry. *Rev. Mod. Phys.*, 79:291–352, Feb 2007.
- [8] S. R. Beane, E. Chang, W. Detmold, H. W. Lin, T. C. Luu, K. Orginos, A. Parreño, M. J. Savage, A. Torok, and A. Walker-Loud. Deuteron and exotic two-body bound states from lattice qcd. *Phys. Rev. D*, 85:054511, Mar 2012.
- [9] Omar Benhar, Nicola Farina, Hiroki Nakamura, Makoto Sakuda, and Ryoichi Seki. Electron- and neutrino-nucleus scattering in the impulse approximation regime. *Phys. Rev. D*, 72:053005, Sep 2005.
- [10] J. Beringer, J. F. Arguin, R. M. Barnett, K. Copic, O. Dahl, D. E. Groom, C. J. Lin, J. Lys, H. Murayama, C. G. Wohl, W. M. Yao, P. A. Zyla, C. Amsler, M. Antonelli, D. M. Asner, H. Baer, H. R. Band, T. Basaglia, C. W. Bauer, J. J. Beatty, V. I. Belousov, E. Bergren, G. Bernardi, W. Bertl, S. Bethke, H. Bichsel, O. Biebel, E. Blucher, S. Blusk, G. Brooijmans, O. Buchmueller, R. N. Cahn, M. Carena, A. Cecucci, D. Chakraborty, M. C. Chen, R. S. Chivukula, G. Cowan, G. D’Ambrosio, T. Damour, D. de Florian, A. de Gouvêa, T. DeGrand, P. de Jong, G. Dissertori, B. Dobrescu, M. Doser, M. Drees, D. A. Edwards, S. Eidelman, J. Erler, V. V. Ezhela, W. Fetscher, B. D. Fields, B. Foster, T. K. Gaisser, L. Garren, H. J. Gerber, G. Gerbier, T. Gherghetta, S. Golwala, M. Goodman, C. Grab, A. V. Gritsan, J. F. Grivaz, M. Grünewald, A. Gurtu, T. Gutsche, H. E. Haber, K. Hagiwara, C. Hagmann, C. Hanhart, S. Hashimoto, K. G. Hayes, M. Heffner, B. Heltsley, J. J. Hernández-Rey, K. Hikasa, A. Höcker, J. Holder, A. Holtkamp, J. Huston, J. D. Jackson, K. F. Johnson, T. Junk, D. Karlen, D. Kirkby, S. R. Klein, E. Klempt, R. V. Kowalewski, F. Krauss, M. Kreps, B. Krusche, Yu. V. Kuyanov, Y. Kwon, O. Lahav, J. Laiho, P. Langacker,

- A. Liddle, Z. Ligeti, T. M. Liss, L. Littenberg, K. S. Lugovsky, S. B. Lugovsky, T. Man-
 nel, A. V. Manohar, W. J. Marciano, A. D. Martin, A. Masoni, J. Matthews, D. Mil-
 stead, R. Miquel, K. Mönig, F. Moortgat, K. Nakamura, M. Narain, P. Nason, S. Navas,
 M. Neubert, P. Nevski, Y. Nir, K. A. Olive, L. Pape, J. Parsons, C. Patrignani, J. A.
 Peacock, S. T. Petcov, A. Piepke, A. Pomarol, G. Punzi, A. Quadt, S. Raby, G. Raf-
 felt, B. N. Ratcliff, P. Richardson, S. Roesler, S. Rolli, A. Romaniouk, L. J. Rosenberg,
 J. L. Rosner, C. T. Sachrajda, Y. Sakai, G. P. Salam, S. Sarkar, F. Sauli, O. Schnei-
 der, K. Scholberg, D. Scott, W. G. Seligman, M. H. Shaevitz, S. R. Sharpe, M. Silari,
 T. Sjöstrand, P. Skands, J. G. Smith, G. F. Smoot, S. Spanier, H. Spieler, A. Stahl,
 T. Stanev, S. L. Stone, T. Sumiyoshi, M. J. Syphers, F. Takahashi, M. Tanabashi,
 J. Terning, M. Titov, N. P. Tkachenko, N. A. Törnqvist, D. Tovey, G. Valencia, K. van
 Bibber, G. Venanzoni, M. G. Vincter, P. Vogel, A. Vogt, W. Walkowiak, C. W. Walter,
 D. R. Ward, T. Watari, G. Weiglein, E. J. Weinberg, L. R. Wiencke, L. Wolfenstein,
 J. Womersley, C. L. Woody, R. L. Workman, A. Yamamoto, G. P. Zeller, O. V. Zenin,
 J. Zhang, R. Y. Zhu, G. Harper, V. S. Lugovsky, and P. Schaffner. Review of particle
 physics. *Phys. Rev. D*, 86:010001, Jul 2012.
- [11] H. A. Bethe. Nuclear many-body problem. *Phys. Rev.*, 103:1353–1390, Sep 1956.
- [12] Sven Binder, Piotr Piecuch, Angelo Calci, Joachim Langhammer, Petr Navrátil, and
 Robert Roth. Extension of coupled-cluster theory with a noniterative treatment of
 connected triply excited clusters to three-body hamiltonians. *Phys. Rev. C*, 88:054319,
 Nov 2013.
- [13] R. M. Bionta, G. Blewitt, C. B. Bratton, D. Casper, A. Ciocio, R. Claus, B. Cortez,
 M. Crouch, S. T. Dye, S. Errede, G. W. Foster, W. Gajewski, K. S. Ganezer, M. Gold-
 haber, T. J. Haines, T. W. Jones, D. Kielczewska, W. R. Kropp, J. G. Learned, J. M.
 LoSecco, J. Matthews, R. Miller, M. S. Mudan, H. S. Park, L. R. Price, F. Reines,
 J. Schultz, S. Seidel, E. Shumard, D. Sinclair, H. W. Sobel, J. L. Stone, L. R. Sulak,
 R. Svoboda, G. Thornton, J. C. van der Velde, and C. Wuest. Observation of a neu-
 trino burst in coincidence with supernova 1987a in the large magellanic cloud. *Phys.*
Rev. Lett., 58:1494–1496, Apr 1987.
- [14] R. F. Bishop, M. F. Flynn, M. C. Boscá, E. Buenda, and R. Guardiola. Translationally
 invariant coupled cluster theory for simple finite systems. *Phys. Rev. C*, 42:1341–1360,
 Oct 1990.
- [15] S. K. Bogner, H. Hergert, J. D. Holt, A. Schwenk, S. Binder, A. Calci, J. Langhammer,
 and R. Roth. Nonperturbative shell-model interactions from the in-medium similarity
 renormalization group. *Phys. Rev. Lett.*, 113:142501, Oct 2014.
- [16] S. K. Bogner, H. Hergert, J. D. Holt, A. Schwenk, S. Binder, A. Calci, J. Langhammer,
 and R. Roth. Nonperturbative shell-model interactions from the in-medium similarity
 renormalization group. *Phys. Rev. Lett.*, 113:142501, Oct 2014.
- [17] S.K. Bogner, R.J. Furnstahl, and A. Schwenk. From low-momentum interactions to
 nuclear structure. *Progress in Particle and Nuclear Physics*, 65(1):94 – 147, 2010.

- [18] Baird H. Brandow. Linked-cluster expansions for the nuclear many-body problem. *Rev. Mod. Phys.*, 39:771–828, Oct 1967.
- [19] L. Brillouin. Les problèmes de perturbations et les champs self-consistents. *Le journal de physique et le radium*, 3(9):373–389, 1932.
- [20] B. A. Brown and B. H. Wildenthal. Corrections to the free-nucleon values of the single-particle matrix elements of the $m1$ and gamow-teller operators, from a comparison of shell-model predictions with sd-shell data. *Phys. Rev. C*, 28:2397–2413, Dec 1983.
- [21] Charles G Broyden. A class of methods for solving nonlinear simultaneous equations. *Math. Comput.*, 19(92):577–593, 1965.
- [22] K. A. Brueckner and C. A. Levinson. Approximate reduction of the many-body problem for strongly interacting particles to a problem of self-consistent fields. *Phys. Rev.*, 97:1344–1352, Mar 1955.
- [23] S. Bustabad, G. Bollen, M. Brodeur, D. L. Lincoln, S. J. Novario, M. Redshaw, R. Ringle, S. Schwarz, and A. A. Valverde. First direct determination of the ^{48}Ca double- β decay q value. *Phys. Rev. C*, 88:022501, Aug 2013.
- [24] Nicola Cabibbo. Unitary symmetry and leptonic decays. *Phys. Rev. Lett.*, 10:531–533, Jun 1963.
- [25] J. Carlson, S. Gandolfi, F. Pederiva, Steven C. Pieper, R. Schiavilla, K. E. Schmidt, and R. B. Wiringa. Quantum monte carlo methods for nuclear physics. *Rev. Mod. Phys.*, 87:1067–1118, Sep 2015.
- [26] J. Cizek and J. Paldus. Correlation problems in atomic and molecular systems iii. rederivation of the coupled-pair many-electron theory using the traditional quantum chemical methodst. *International Journal of Quantum Chemistry*, 5(4):359–379, 1971.
- [27] J. Cizek and J. Paldus. Coupled cluster approach. *Physica Scripta*, 21(3-4):251, 1980.
- [28] Jiri Cizek. On the correlation problem in atomic and molecular systems. calculation of wavefunction components in urselltype expansion using quantumfield theoretical methods. *The Journal of Chemical Physics*, 45(11):4256–4266, 1966.
- [29] D. B. Cline, G. M. Fuller, W. P. Hong, B. Meyer, and J. Wilson. Prospects for detection of a cosmologically significant neutrino mass from a galactic supernova neutrino burst using a neutral-current-based detector. *Phys. Rev. D*, 50:720–729, Jul 1994.
- [30] F. Coester. Bound states of a many-particle system. *Nuclear Physics*, 7(Supplement C):421 – 424, 1958.
- [31] F. Coester and H. Kmmel. Short-range correlations in nuclear wave functions. *Nuclear Physics*, 17(Supplement C):477 – 485, 1960.
- [32] E. U. Condon. The theory of complex spectra. *Phys. Rev.*, 36:1121–1133, Oct 1930.

- [33] E. U. Condon. The theory of complex spectra. *Phys. Rev.*, 36:1121–1133, Oct 1930.
- [34] Geerd H.F. Diercksen, Björn O. Roos, and Andrzej J. Sadlej. Legitimate calculation of first-order molecular properties in the case of limited ci functions. dipole moments. *Chemical Physics*, 59(1):29 – 39, 1981.
- [35] A. Ekström, G. R. Jansen, K. A. Wendt, G. Hagen, T. Papenbrock, S. Bacca, B. Carlsson, and D. Gazit. Effects of three-nucleon forces and two-body currents on gamow-teller strengths. *Phys. Rev. Lett.*, 113:262504, Dec 2014.
- [36] S. R. Elliott, A. A. Hahn, and M. K. Moe. Direct evidence for two-neutrino double-beta decay in ^{82}Se . *Phys. Rev. Lett.*, 59:2020–2023, Nov 1987.
- [37] Jonathan Engel. Nuclear matrix elements for double- β decay. *XXVI International Conference on Neutrino Physics and Astrophysics (Neutrino 2014)*, 1666, 2015.
- [38] D. R. Entem and R. Machleidt. Accurate charge-dependent nucleon-nucleon potential at fourth order of chiral perturbation theory. *Phys. Rev. C*, 68:041001, Oct 2003.
- [39] E. Epelbaum, H.-W. Hammer, and Ulf-G. Meißner. Modern theory of nuclear forces. *Rev. Mod. Phys.*, 81:1773–1825, Dec 2009.
- [40] M. Ernzerhof, C.M. Marian, and S.D. Peyerimhoff. Energy derivative versus expectation value approach: the dipole moment of co. *Chemical Physics Letters*, 204(1):59 – 64, 1993.
- [41] G.T. Ewan. The sudbury neutrino observatory. *Nuclear Instruments and Methods in Physics Research Section A: Accelerators, Spectrometers, Detectors and Associated Equipment*, 314(2):373 – 379, 1992.
- [42] E. Fermi. Versuch einer Theorie der β -Strahlen. I. *Zeitschrift für Physik*, 88:161–177, March 1934.
- [43] A.L. Fetter and J.D. Walecka. *Quantum Theory of Many-particle Systems*. Dover Books on Physics. Dover Publications, 2003.
- [44] V. Fock. Näherungsmethode zur lösung des quantenmechanischen mehrkörperproblems. *Zeitschrift für Physik*, 61(1):126–148, Jan 1930.
- [45] Lee M. Frantz and Robert L. Mills. Many-body basis for the optical model. *Nuclear Physics*, 15:16 – 32, 1960.
- [46] D.H. Gloeckner and R.D. Lawson. Spurious center-of-mass motion. *Physics Letters B*, 53(4):313 – 318, 1974.
- [47] J. R. Gour, P. Piecuch, M. Hjorth-Jensen, M. Włoch, and D. J. Dean. Coupled-cluster calculations for valence systems around ^{16}O . *Phys. Rev. C*, 74:024310, Aug 2006.
- [48] E. K. U. Gross, E. Runge, and O. Heinonen. *Many-particle theory / E.K.U. Gross, E. Runge, O. Heinonen*. A. Hilger Bristol ; Philadelphia, 1991.

- [49] K. Gulyuz, J. Ariche, G. Bollen, S. Bustabad, M. Eibach, C. Izzo, S. J. Novario, M. Redshaw, R. Ringle, R. Sandler, S. Schwarz, and A. A. Valverde. Determination of the direct double- β -decay q value of ^{96}Zr and atomic masses of $^{90-92,94,96}\text{Zr}$ and $^{92,94-98,100}\text{Mo}$. *Phys. Rev. C*, 91:055501, May 2015.
- [50] G. Hagen, D.J. Dean, M. Hjorth-Jensen, and T. Papenbrock. Complex coupled-cluster approach to an ab-initio description of open quantum systems. *Physics Letters B*, 656(4):169 – 173, 2007.
- [51] G. Hagen, A. Ekström, C. Forssén, G. R. Jansen, W. Nazarewicz, T. Papenbrock, K. A. Wendt, S. Bacca, N. Barnea, B. Carlsson, C. Drischler, K. Hebeler, M. Hjorth-Jensen, M. Miorelli, G. Orlandini, A. Schwenk, and J. Simonis. Neutron and weak-charge distributions of the ^{48}Ca nucleus. *Nature Physics*, 12:186 EP –, Nov 2015. Article.
- [52] G. Hagen, T. Papenbrock, and D. J. Dean. Solution of the center-of-mass problem in nuclear structure calculations. *Phys. Rev. Lett.*, 103:062503, Aug 2009.
- [53] G. Hagen, T. Papenbrock, M. Hjorth-Jensen, and D. J. Dean. Coupled-cluster computations of atomic nuclei. *Rep. Prog. in Phys.*, 77(9):096302, Sep 2014.
- [54] J. C. Hardy and I. S. Towner. Superaligned $0^+ \rightarrow 0^+$ nuclear β decays: A critical survey with tests of the conserved vector current hypothesis and the standard model. *Phys. Rev. C*, 71:055501, May 2005.
- [55] C.K. Hargrove, I. Batkin, M.K. Sundaresan, and J. Dubeau. A lead astronomical neutrino detector: Land. *Astroparticle Physics*, 5(2):183 – 196, 1996.
- [56] D. R. Hartree. The wave mechanics of an atom with a non-coulomb central field. part i. theory and methods. *Mathematical Proceedings of the Cambridge Philosophical Society*, 24(1):89110, 1928.
- [57] H Hergert. In-medium similarity renormalization group for closed and open-shell nuclei. *Physica Scripta*, 92(2):023002, 2017.
- [58] H. Hergert, S. Binder, A. Calci, J. Langhammer, and R. Roth. Ab initio calculations of even oxygen isotopes with chiral two-plus-three-nucleon interactions. *Phys. Rev. Lett.*, 110:242501, Jun 2013.
- [59] H. Hergert, S. K. Bogner, T. D. Morris, S. Binder, A. Calci, J. Langhammer, and R. Roth. Ab initio multireference in-medium similarity renormalization group calculations of even calcium and nickel isotopes. *Phys. Rev. C*, 90:041302, Oct 2014.
- [60] Heiko Hergert. Private communication.
- [61] K. Hirata, T. Kajita, M. Koshiba, M. Nakahata, Y. Oyama, N. Sato, A. Suzuki, M. Takita, Y. Totsuka, T. Kifune, T. Suda, K. Takahashi, T. Tanimori, K. Miyano, M. Yamada, E. W. Beier, L. R. Feldscher, S. B. Kim, A. K. Mann, F. M. Newcomer, R. Van, W. Zhang, and B. G. Cortez. Observation of a neutrino burst from the supernova sn1987a. *Phys. Rev. Lett.*, 58:1490–1493, Apr 1987.

- [62] J. Hubbard. The description of collective motions in terms of many-body perturbation theory. *Proceedings of the Royal Society of London. Series A, Mathematical and Physical Sciences*, 240(1223):539–560, 1957.
- [63] N.M. Hugenholtz. Perturbation theory of large quantum systems. *Physica*, 23(1):481 – 532, 1957.
- [64] G. R. Jansen. Spherical coupled-cluster theory for open-shell nuclei. *Phys. Rev. C*, 88:024305, Aug 2013.
- [65] G. R. Jansen, J. Engel, G. Hagen, P. Navrátil, and A. Signoracci. Ab-initio coupled-cluster effective interactions for the shell model: Application to neutron-rich oxygen and carbon isotopes. *Phys. Rev. Lett.*, 113:142502, Oct 2014.
- [66] G. R. Jansen, M. D. Schuster, A. Signoracci, G. Hagen, and P. Navrátil. Open *sd*-shell nuclei from first principles. *Phys. Rev. C*, 94:011301, Jul 2016.
- [67] W. Jaus and G. Rasche. Nuclear-structure dependence of $o(\alpha)$ corrections to fermi decays and the value of the kobayashi-maskawa matrix element V_{ud} . *Phys. Rev. D*, 41:166–176, Jan 1990.
- [68] Makoto Kobayashi and Toshihide Maskawa. Cp-violation in the renormalizable theory of weak interaction. *Progress of Theoretical Physics*, 49(2):652–657, 1973.
- [69] E Kolbe, K Langanke, G Martinez-Pinedo, and P Vogel. Neutrinonucleus reactions and nuclear structure. *Journal of Physics G: Nuclear and Particle Physics*, 29(11):2569, 2003.
- [70] K. Kowalski, D. J. Dean, M. Hjorth-Jensen, T. Papenbrock, and P. Piecuch. Coupled cluster calculations of ground and excited states of nuclei. *Phys. Rev. Lett.*, 92:132501, Apr 2004.
- [71] H. Kmmel, K.H. Lhrmann, and J.G. Zabolitzky. Many-fermion theory in exps- (or coupled cluster) form. *Physics Reports*, 36(1):1 – 63, 1978.
- [72] K. Langanke, P. Vogel, and E. Kolbe. Signal for supernova ν_μ and ν_τ neutrinos in water Čerenkov detectors. *Phys. Rev. Lett.*, 76:2629–2632, Apr 1996.
- [73] David L. Lincoln, Jason D. Holt, Georg Bollen, Maxime Brodeur, Scott Bustabad, Jonathan Engel, Samuel J. Novario, Matthew Redshaw, Ryan Ringle, and Stefan Schwarz. First direct double- β decay q -value measurement of ^{82}Se in support of understanding the nature of the neutrino. *Phys. Rev. Lett.*, 110:012501, Jan 2013.
- [74] H. J. Lipkin. Center-of-mass motion in the nuclear shell model. *Phys. Rev.*, 110:1395–1397, Jun 1958.
- [75] P. López Ríos, A. Ma, N. D. Drummond, M. D. Towler, and R. J. Needs. Inhomogeneous backflow transformations in quantum monte carlo calculations. *Phys. Rev. E*, 74:066701, Dec 2006.

- [76] R. Machleidt and D.R. Entem. Chiral effective field theory and nuclear forces. *Physics Reports*, 503(1):1 – 75, 2011.
- [77] Ruprecht Machleidt. Chiral symmetry and the nucleon-nucleon interaction. *Symmetry*, 8(4), 2016.
- [78] N. Michel, W. Nazarewicz, M. Płoszajczak, and J. Rotureau. Antibound states and halo formation in the gamow shell model. *Phys. Rev. C*, 74:054305, Nov 2006.
- [79] H. S. Miley, F. T. Avignone, R. L. Brodzinski, J. I. Collar, and J. H. Reeves. Suggestive evidence for the two-neutrino double- β decay of ^{76}Ge . *Phys. Rev. Lett.*, 65:3092–3095, Dec 1990.
- [80] Nimrod Moiseyev. *Non-Hermitian Quantum Mechanics*. Cambridge University Press, 2011.
- [81] Chr. Møller and M. S. Plesset. Note on an approximation treatment for many-electron systems. *Phys. Rev.*, 46:618–622, Oct 1934.
- [82] P. Navrátil. Local three-nucleon interaction from chiral effective field theory. *Few-Body Systems*, 41(3):117–140, Dec 2007.
- [83] P. Navrátil, J. P. Vary, and B. R. Barrett. Large-basis ab initio no-core shell model and its application to ^{12}C . *Phys. Rev. C*, 62:054311, Oct 2000.
- [84] Petr Navrátil, Sofia Quaglioni, Ionel Stetcu, and Bruce R Barrett. Recent developments in no-core shell-model calculations. *Journal of Physics G: Nuclear and Particle Physics*, 36(8):083101, 2009.
- [85] A. Nogga, H. Kamada, W. Glöckle, and B. R. Barrett. The α particle based on modern nuclear forces. *Phys. Rev. C*, 65:054003, May 2002.
- [86] W. E. Ormand and B. A. Brown. Isospin-mixing corrections for fp-shell fermi transitions. *Phys. Rev. C*, 52:2455–2460, Nov 1995.
- [87] Piotr Piecuch, Karol Kowalski, Ian S. O. Pimienta, and Michael J. McGuire. Recent advances in electronic structure theory: Method of moments of coupled-cluster equations and renormalized coupled-cluster approaches. *International Reviews in Physical Chemistry*, 21(4):527–655, 2002.
- [88] Steven C. Pieper, , and R. B. Wiringa. Quantum monte carlo calculations of light nuclei. *Annual Review of Nuclear and Particle Science*, 51(1):53–90, 2001.
- [89] B. S. Pudliner, V. R. Pandharipande, J. Carlson, Steven C. Pieper, and R. B. Wiringa. Quantum monte carlo calculations of nuclei with $a \leq 7$. *Phys. Rev. C*, 56:1720–1750, Oct 1997.
- [90] P. Pulay. Improved scf convergence acceleration. *J. Comput. Chem.*, 3(4):556–560, 1982.

- [91] Péter Pulay. Convergence acceleration of iterative sequences. the case of scf iteration. *Chem. Phys. Lett.*, 73(2):393 – 398, 1980.
- [92] Matthew Redshaw, Georg Bollen, Maxime Brodeur, Scott Bustabad, David L. Lincoln, Samuel J. Novario, Ryan Ringle, and Stefan Schwarz. Atomic mass and double- β -decay q value of ^{48}Ca . *Phys. Rev. C*, 86:041306, Oct 2012.
- [93] Robert Roth, Sven Binder, Klaus Vobig, Angelo Calci, Joachim Langhammer, and Petr Navrátil. Medium-mass nuclei with normal-ordered chiral $nn+3n$ interactions. *Phys. Rev. Lett.*, 109:052501, Jul 2012.
- [94] Robert Roth, Joachim Langhammer, Angelo Calci, Sven Binder, and Petr Navrátil. Similarity-transformed chiral $nn + 3n$ interactions for the ab initio description of ^{12}C and ^{16}O . *Phys. Rev. Lett.*, 107:072501, Aug 2011.
- [95] H.F. Schaefer. *Quantum chemistry: the development of ab initio methods in molecular electronic structure theory*. Oxford science publications. Clarendon Press, 1984.
- [96] Meiyue Shao, Hasan Metin Aktulga, Chao Yang, Esmond G. Ng, Pieter Maris, and James P. Vary. Accelerating nuclear configuration interaction calculations through a preconditioned block iterative eigensolver. *CoRR*, abs/1609.01689, 2016.
- [97] I. Shavitt and R. J. Bartlett. *Many-Body Methods in Chemistry and Physics: MBPT and Coupled-Cluster Theory*. Cambridge Molecular Science. Cambridge University Press, 2009.
- [98] C. David Sherrill and Henry F. Schaefer. The configuration interaction method: Advances in highly correlated approaches. volume 34 of *Advances in Quantum Chemistry*, pages 143 – 269. Academic Press, 1999.
- [99] J. C. Slater. The theory of complex spectra. *Phys. Rev.*, 34:1293–1322, Nov 1929.
- [100] J. C. Slater. The theory of complex spectra. *Phys. Rev.*, 34:1293–1322, Nov 1929.
- [101] V. Somà, C. Barbieri, and T. Duguet. Ab initio gorkov-green’s function calculations of open-shell nuclei. *Phys. Rev. C*, 87:011303, Jan 2013.
- [102] V. Somà, C. Barbieri, and T. Duguet. Ab initio self-consistent gorkov-green’s function calculations of semi-magic nuclei: Numerical implementation at second order with a two-nucleon interaction. *Phys. Rev. C*, 89:024323, Feb 2014.
- [103] V. Somà, A. Cipollone, C. Barbieri, P. Navrátil, and T. Duguet. Chiral two- and three-nucleon forces along medium-mass isotope chains. *Phys. Rev. C*, 89:061301, Jun 2014.
- [104] S. R. Stroberg, A. Calci, H. Hergert, J. D. Holt, S. K. Bogner, R. Roth, and A. Schwenk. Nucleus-dependent valence-space approach to nuclear structure. *Phys. Rev. Lett.*, 118:032502, Jan 2017.

- [105] S. R. Stroberg, H. Hergert, J. D. Holt, S. K. Bogner, and A. Schwenk. Ground and excited states of doubly open-shell nuclei from ab initio valence-space hamiltonians. *Phys. Rev. C*, 93:051301, May 2016.
- [106] Jouni Suhonen and Osvaldo Civitarese. Weak-interaction and nuclear-structure aspects of nuclear double beta decay. *Physics Reports*, 300(3):123 – 214, 1998.
- [107] Jouni Suhonen and Osvaldo Civitarese. Probing the quenching of ga by single and double beta decays. *Physics Letters B*, 725(1):153 – 157, 2013.
- [108] Pter Szakcs and Pter R. Surjn. Stability conditions for the coupled cluster equations. *International Journal of Quantum Chemistry*, 108(12):2043–2052, 2008.
- [109] D.J. Thouless. Stability conditions and nuclear rotations in the hartree-fock theory. *Nuclear Physics*, 21:225 – 232, 1960.
- [110] I S Towner and J C Hardy. The evaluation of v_{ud} , experiment and theory. *Journal of Physics G: Nuclear and Particle Physics*, 29(1):197, 2003.
- [111] I. S. Towner and J. C. Hardy. An Improved calculation of the isospin-symmetry-breaking corrections to superallowed Fermi beta decay. *Phys. Rev.*, C77:025501, 2008.
- [112] I. S. Towner and F. C. Khanna. Quenching of allowed gamow-teller β transitions in mirror nuclei. *Phys. Rev. Lett.*, 42:51–54, Jan 1979.
- [113] I.S. Towner. The nuclear-structure dependence of radiative corrections in superallowed fermi beta-decay. *Nuclear Physics A*, 540(3):478 – 500, 1992.
- [114] I.S. Towner. Quenching of spin operators in the calculation of radiative corrections for nuclear beta decay. *Physics Letters B*, 333(1):13 – 16, 1994.
- [115] K. Tsukiyama, S. K. Bogner, and A. Schwenk. In-medium similarity renormalization group for nuclei. *Phys. Rev. Lett.*, 106:222502, Jun 2011.
- [116] K. Tsukiyama, S. K. Bogner, and A. Schwenk. In-medium similarity renormalization group for open-shell nuclei. *Phys. Rev. C*, 85:061304, Jun 2012.
- [117] C. W. Ufford. Configuration interaction in complex spectra. *Phys. Rev.*, 44:732–739, Nov 1933.
- [118] C. M. Vincent. Optimal separation of center-of-mass motion. *Phys. Rev. C*, 8:929–937, Sep 1973.
- [119] E. K. Warburton and B. A. Brown. Effective interactions for the 0p1s0d nuclear shell-model space. *Phys. Rev. C*, 46:923–944, Sep 1992.
- [120] G. C. Wick. The evaluation of the collision matrix. *Phys. Rev.*, 80:268–272, Oct 1950.
- [121] B. H. Wildenthal, M. S. Curtin, and B. A. Brown. Predicted features of the beta decay of neutron-rich sd-shell nuclei. *Phys. Rev. C*, 28:1343–1366, Sep 1983.

- [122] Fred L. Wilson. Fermi's theory of beta decay. *American Journal of Physics*, 36(12):1150–1160, 1968.
- [123] M. Włoch, D. J. Dean, J. R. Gour, M. Hjorth-Jensen, K. Kowalski, T. Papenbrock, and P. Piecuch. Ab-initio coupled-cluster study of ^{16}O . *Phys. Rev. Lett.*, 94:212501, Jun 2005.
- [124] Marta Woch, Jeffrey R Gour, Piotr Piecuch, David J Dean, Morten Hjorth-Jensen, and Thomas Papenbrock. Coupled-cluster calculations for ground and excited states of closed- and open-shell nuclei using methods of quantum chemistry. *Journal of Physics G: Nuclear and Particle Physics*, 31(8):S1291, 2005.
- [125] Tomislav P. Ivković. Existence and reality of solutions of the coupled-cluster equations. *International Journal of Quantum Chemistry*, 12(S11):413–420, 1977.